Non-invasive multiphoton imaging of neural structure and activity in *Drosophila*

Max Jameson Aragon[1,5,#], Mengran Wang[2,#], Jamien Shea[1], Aaron T. Mok[2], Haein Kim[1], Kawasi M. Lett[3], Nathan Barkdull[4], Chris B. Schaffer[3], Chris Xu[2] and Nilay Yapici[1,*]

[1]*Department of Neurobiology and Behaviour, Cornell University, 14853, Ithaca, NY, USA*
[2]*School of Applied and Engineering Physics, Cornell University, 14853, Ithaca, NY, USA*
[3]*The Meinig School of Biomedical Engineering, Cornell University, 14853, Ithaca, NY, USA*
[4]*Department of Physics, University of Florida, 32611, Gainesville, FL, USA*
[5]*Current address: Princeton Neuroscience Institute, Princeton University, 08544, Princeton, NJ, USA*

[#]*These authors contributed equally to this work*
**Corresponding author: Nilay Yapici (ny96@cornell.edu)*

Abstract

A limitation of current methods for examining neural activity over long periods of time in the fly, *Drosophila melanogaster,* is the need to remove the head cuticle and the underlying tissue to gain optical access to the brain, a process that damages circulation and restricts the length of imaging time. Here, we developed a non-invasive preparation for structural and functional imaging of the fly brain through the intact head cuticle. We first showed that the head cuticle transmits long-wavelength laser light with surprisingly high efficiencies. In fact, the tissue that interferes with laser light during multiphoton imaging is the air sacs underneath the head cuticle. We developed a non-invasive imaging preparation that compresses the air sacs, and used it to image the mushroom body Kenyon cells and central complex ring neurons through the cuticle at cellular resolution using both 2-and 3-photon microscopy. We also performed non-invasive short-term and long-term functional imaging (for the first time for 12 consecutive hours) of odour-evoked calcium responses from the mushroom body Kenyon cells. Our results demonstrate that the non-invasive imaging preparation developed here extends the time limits of current *in vivo* imaging methods used in flies that require an invasive surgery, and opens up new ways to capture neural activity from the intact fly brain.

Main

Animal nervous systems across lineages have evolved to solve many of the same problems, such as foraging for food and water, finding mates to reproduce, and avoiding predators to stay alive. They navigate their environment via coordinated movements, and learn and remember the relative values of sensory stimuli around them in order to maximize their fitness and survival. At each instant in time, an animal must evaluate external sensory information and its current behavioural state to decide what to do next [1-6]. A major technological challenge to revealing how the brain encodes behavioural states in real-time is that even the simplest neural computation involves interactions across the nervous system at various time scales, while our tools for assessing neural activity are restricted in time and space because of the currently available imaging sensors, methods, and preparations [7]. Optical methods remain the most established and fruitful path for revealing population dynamics in neural circuits at long time scales (ranging from minutes to hours) by providing high temporal and spatial resolution measurements [8-10].

The fly, *Drosophila melanogaster*, offers an ideal experimental system to investigate neural correlates of behavioural states and decisions because of its compact nervous system and diverse state-dependent behaviours that it executes in response to sensory stimuli [4, 11, 12]. To understand how molecularly defined neural circuits evaluate sensory information in different behavioural states, it is critical to capture the activity of populations of neurons over long time scales as flies are changing their physiological needs [8, 13]. These functional imaging experiments require non-invasive imaging preparations, which should allow chronic neural activity imaging for at least 12 to 24 hours. Current methods used in fly optical physiology require the fly head cuticle, trachea, and fat body to be removed by microsurgery to provide optical access to the nervous system [14-18]. These preparations are limited in imaging duration because after some time, the brain tissue starts dying due to damaged circulation resulting from the cuticle removal surgery. For example, with current imaging preparations, fly olfactory neurons show reliable Ca^{2+} responses for about four to five

53 hours after surgery [18]. A non-invasive imaging method and a preparation in which the head cuticle
54 and underlying tissue are left intact, thereby eliminating the need for traumatic head surgery before
55 functional imaging, is essential for advancing fly neuroscience research in the direction of chronic
56 recordings of neural activity during ongoing behaviours. This includes being able to image the
57 same fly brain across multiple days. In mice, multi-day imaging experiments are achieved by
58 implanting a cranial window following removal of part of the skull [19, 20]. Similar imaging
59 preparations have been developed for flies [14, 16, 21]. However, because imaging window
60 implantation requires a tedious surgery with low success rates and complications that occur
61 afterwards, these methods are not commonly used.

62 A recent development in *in vivo* multiphoton imaging is the use of long wavelength lasers in
63 3-photon (3P) microscopy which improves the signal-to-background ratio by several orders of
64 magnitude compared to current 2-photon (2P) imaging methods [22-24]. For example, 3P excitation at
65 1300 nm allows the functional imaging of neurons labelled with a genetically encoded Ca^{2+}
66 indicator GCaMP6 in the CA1 hippocampal region in an intact mouse brain [24, 25]. Recently, 3P
67 microscopy at 1700 nm excitation has shown promising results in imaging the fly brain through the
68 cuticle [26].

69 Here, we developed a non-invasive imaging preparation for flies to image neural structure
70 and activity through the intact head cuticle with both 2P and 3P microscopy. We first measured the
71 ballistic and total optical transmission of long-wavelength lasers through the dorsal fly head cuticle
72 and surprisingly found that the cuticle has high transmission at the wavelengths that are used to
73 excite fluorophores in 2P and 3P microscopy. We showed that the tissue that interferes with the
74 laser light and limits imaging through the cuticle into the brain is not the head cuticle but the air
75 sacs and the trachea underneath the cuticle. Next, we developed a new imaging preparation that
76 mildly compresses the air sacs and allows non-invasive imaging of the fly brain without any
77 surgery. Using this imaging preparation, we captured neural structures of mushroom body Kenyon

78 cells and the central complex ring neurons with cellular resolution at 910 nm (2P) and 1320 nm
79 (3P) excitation. We also performed short-term and long-term functional imaging of odour-evoked
80 neural activity of Kenyon cells comprising the mushroom body γ-lobes using a genetically encoded
81 Ca^{2+} indicator, GCaMP6s [27]. Kenyon cells are the primary intrinsic neurons in the insect mushroom
82 body. Diverse subtypes of Kenyon cells (n=~2200) extend their axons along the pedunculus and in
83 the dorsal and medial lobes [28-30]. These neurons receive and integrate information from
84 heterogeneous sets of projection neurons which carry olfactory, gustatory, and visual sensory
85 information [31, 32]. In our chronic 3P functional imaging experiments, we found that odour evoked
86 Ca^{2+} responses in the mushroom body γ-lobes change with time.

87 Our non-invasive imaging preparation developed here for the first time allows 2P and 3P
88 structural and functional imaging of the fly brain without any microsurgery, opening a door to
89 capturing neural activity at long time scales and potentially through the entire lifespan of flies.
90 Ultimately, we expect that our results will push forward the current methods that are used for
91 anatomical and functional imaging of the adult fly nervous system *in vivo*.

92 Results

93 Fly head cuticle transmits long wavelength laser light with high efficiency

94 To develop a non-invasive imaging preparation using multiphoton microscopy, we first tested the
95 transmission of infrared wavelengths through the fly head cuticle. Previous experiments showed
96 that the dorsal head cuticle of *Drosophila melanogaster* transmits light with increased efficiency at
97 longer wavelengths [33]. We measured the total and ballistic transmission of infrared wavelengths
98 through the cuticle. Dissected head cuticle samples were mounted between two glass coverslips,
99 and placed in the beam path between the laser source and the photodetector (Fig. 1a). The total and
100 ballistic transmission through the cuticle samples were measured using a custom-built system (Fig.
101 1b). For ballistic transmission, light from a single-mode fibre was magnified and focused on the
102 cuticle with a ~25µm spot size. Fig. 1c illustrates the light path of ballistic transmission

103 experiments. The sample was moved around to obtain measurements at different locations on the
104 same sample. Ballistic transmission through the cuticle was measured at seven different
105 wavelengths (852 nm, 915 nm, 980 nm, 1054 nm, 1310 nm, 1510 nm, 1630 nm). Our results
106 showed that ballistic transmission of the laser light through the cuticle samples increased with laser
107 wavelength (Fig. 1d). At all of the laser wavelengths tested, the ballistic transmission through the
108 cuticle was surprisingly high, reaching up to >90% at 1310 nm (Fig. 1d). The fluorescence signal
109 within the focal volume in 2P- and 3P-microscopy is mostly generated by the ballistic photons.

110 Next, we measured the total transmission through the head cuticle. For these measurements,
111 laser light from a single mode fibre was magnified and focused on the cuticle sample with a ~50µm
112 spot size. An integrating sphere was placed immediately after the cuticle to measure the total laser
113 transmission. Fig. 1e illustrates the light path of total transmission experiments. Total transmission
114 through the cuticle was measured at nine different wavelengths (532 nm, 633 nm, 852 nm, 915 nm,
115 980 nm, 1054 nm, 1310 nm, 1510 nm, 1630 nm). Similar to the ballistic transmission experiments,
116 we found that the total transmission increases with wavelength, reaching a plateau around 915 nm
117 (Fig. 1f). The total transmission at shorter wavelengths, 532 nm and 633 nm, was also relatively
118 high (>60%) which is critical for collecting emitted fluorescence produced by green (532 nm) and
119 red (633 nm) fluorophores after 2P or 3P excitation. Our results demonstrated that absorption of
120 long wavelength laser light by the *Drosophila* head cuticle is minimal, suggesting non-invasive
121 excitation of green (GFP, GCaMP) and red fluorophores (RFP, RCaMP) through the cuticle is
122 possible in adult flies using 2P or 3P excitation *in vivo*.

123 **2P and 3P excitation allows non-invasive structural imaging of the fly brain**

124 Based on our results for cuticle transmission, we next used a non-invasive imaging preparation and
125 a custom-built multiphoton microscope equipped with a wavelength-tuneable 2P and 3P laser
126 system to image the fly brain in head-fixed flies *in vivo* (Fig. 2a, Methods). We developed three
127 types of non-invasive imaging preparations with different head compression levels: no

128 compression, semi-compression, and full-compression (Fig. 2b-2d, Methods). As a proof of
129 principle experiment, we expressed membrane tagged GFP selectively in mushroom body Kenyon
130 cells and imaged the fly brain through the cuticle using 2P and 3P excitation at 910 nm and 1320
131 nm laser wavelengths, respectively (Fig. 2e-2g). Mushroom body Kenyon cells are bilaterally
132 symmetric groups of neurons that are subdivided according to their axonal trajectories. The cell
133 bodies of these neurons are located around the calyx of the mushroom bodies. Kenyon cell
134 dendrites arborize in the calyx, while their axons fasciculate into anatomically distinct structures
135 called lobes, with the dorsal lobes forming α and α′ branches, and the medial lobes containing β, β′,
136 and γ branches [29, 30, 34]. We used transgenic flies that specifically expressed GFP in Kenyon cells
137 forming α, β and γ lobes [35]. Using both 2P and 3P excitation, we were able to visualize different
138 anatomical compartments of the fly mushroom body. In non-compressed flies, the mushroom body
139 lobes were barely visible in both 2P and 3P imaged flies. Compressing the head against the glass
140 with forceps during the curing process drastically improved image quality (Fig. 2e-2g,
141 Supplementary video 1 & 2). Flies behaved healthier (based on observations of the leg movement)
142 in semi-compressed preps compared to full-compressed preps, thus we used semi-compressed
143 preps in all further structural and functional imaging experiments with 2P and 3P excitation.
144 We also investigated why head compression improves image quality in intact flies. Our
145 hypothesis is that head compression reduces the volume of the air sacs and surrounding tissue,
146 allowing better transmission of the long wavelength laser light through the structures underneath
147 the head cuticle including dorsal air sacs and other tracheal branches. To test our hypothesis, we
148 surgically removed air sacs from one side of the fly head and imaged the brain using 2P and 3P
149 excitation without any head compression. As predicted, in both 2P and 3P imaged flies, we were
150 able to see the mushroom body lobes on the side where air sacs were removed but not on the side
151 with intact air sacs (Supplementary Fig. 1a-1c, Supplementary video 3). Our results clearly showed
152 that the tissue that interferes with 2P and 3P laser light is not the cuticle itself but the air sacs and

153 the other tissues that are underneath the head cuticle. In parallel to our findings, a recent study also
154 showed that deflating the trachea within the fly brain increases the maximal imaging depth of
155 multiphoton microscopy [36].

156 **3P non-invasive imaging of mushroom body Kenyon cells and central complex ring neurons**
157 **at cellular resolution.**

158 Our non-invasive imaging experiments showed that through–cuticle imaging is possible with both
159 2P and 3P excitation. For further detailed structural imaging experiments, we used 3P excitation at
160 1320 nm. We imaged different anatomical compartments of the mushroom body Kenyon cells and
161 central complex ring neurons at cellular resolution (Fig. 3). We started acquiring images from the
162 deepest structures we could detect in the brain (depth=~150 µm), then moved to shallower areas in
163 ~0.5 µm depth increments and ended imaging outside of the head cuticle (Fig. 3a-3e). In the flies
164 expressing membrane tagged GFP specifically in the mushroom body Kenyon cells, we were able
165 to visualize the calyx and axonal tracts along the peduncle as well as the dorsal and medial lobes
166 containing α, β and γ branches, respectively (Fig. 3a-3b,). In addition to the fluorescence signal,
167 adipose, epithelial-like tissues, and tracheal branches surrounding the mushroom body lobes
168 produced a bright Third Harmonic Generation (THG) signal (yellow) [37]. The tracheal branches
169 were most apparent near the medial lobes at 96 µm depth (Fig. 3a, mid panel). When we focused on
170 the calyx region at higher magnification using a compressed imaging prep with the posterior brain
171 positioned closer to the objective lens, we were also able to distinguish single Kenyon cell bodies,
172 which are densely packed around the calyx (Fig. 3c).

173 Next, we imaged the central complex, another higher order processing centre, that is located
174 in the dorsal and medial part of the fly brain (Fig. 3d-3g). The insect central complex is highly
175 interconnected brain neuropil which processes sensory information and guides a diverse set of
176 behavioural responses which include navigation, walking initiation, and turning direction [38-40]. It is
177 composed of functionally distinct, but anatomically connected, compartments: the protocerebral

178 bridge, ellipsoid body, fan-shaped body, and the paired noduli [38]. The ellipsoid body consists of a
179 group of neurons, the ring neurons, that extend their axons to the midline and form a ring-like
180 structure that is composed of different layers [38, 39, 41]. Using an ellipsoid body-specific promoter, we
181 expressed membrane tagged GFP in the fly brain and imaged the ring neurons through the cuticle at
182 1320 nm (Supplementary video 4 & 5). Ring neuron cell bodies, as well as the lateral triangle and
183 the ellipsoid body layers, were clearly visible (Fig. 3d & 3e). Using ring neuron arbours and
184 tracheal branches, we estimated the lateral resolution of our 3P images. The full width at half
185 maximum (FWHM) of the lateral brightness distribution measured by a ring neuron's neurite cross
186 section was ~1.24 µm for the fluorescent signal (Fig. 3f) and ~0.79 µm for tracheal branches
187 captured by the THG signal (Fig. 3g). We were also able to image the ellipsoid body neuropil with
188 2P excitation through the cuticle. Compared with 3P excitation, the resolution and contrast in
189 images taken by 2P excitation is somewhat reduced in the semi-compressed preparation
190 (Supplementary Fig. 2a & 2b). We also repeated our 3P imaging experiments using a fibre laser-
191 amplifier system with an integrated infrared optical parametric amplifier (OPA, KM Labs). The
192 results using this low power laser system are comparable to what we have obtained previously
193 (Supplementary Fig. 3a & 3b), indicating that a more compact, less powerful laser source is
194 adequate for imaging fly brain structures with 3P microscopy.

195 Our results demonstrate that non-invasive 3P microscopy is able to capture single neurons
196 and fine anatomical structures within the mushroom body and central complex with comparable
197 resolution to the open cuticle preparations using 2P microscopy [18].

198 **Simultaneous 2P and 3P imaging of odour-evoked responses of mushroom body Kenyon cells**
199 **through the head cuticle**

200 Encouraged by our structural imaging results, we next tested the applicability of 2P and 3P
201 microscopy to capture neural activity in the fly brain through the intact head cuticle. In these
202 experiments, a custom odour delivery and behaviour system was used, where flies were head fixed

203 on a polymer ball under the microscope (Fig. 4a-4c). We expressed GCaMP6s selectively in
204 Kenyon cells and stimulated the fly olfactory sensory organ, the antenna, with the food odour apple
205 cider vinegar (Fig. 4b). Using a multiphoton scanning microscope, odour evoked Ca^{2+} responses of
206 mushroom body γ-lobes were simultaneously captured with 2P (910 nm) and 3P (1320 nm)
207 excitation using temporal multiplexing and the semi-compressed imaging prep (Fig. 4a-4e,
208 methods). A brief 3s odour stimulus triggered a robust fluorescence increase in Kenyon cell axons
209 comprising the mushroom body γ-lobes (Fig. 4f, Supplementary video 6). Kenyon cell axons are
210 innervated by distinct subsets of dopaminergic neurons, which carry contextual information to the
211 mushroom body depending on the fly's previous experiences. Based on dopaminergic innervation,
212 γ-lobes can be subdivided into five anatomical compartments [42] (Fig. 4d & 4e). To determine
213 whether the localized dopaminergic input along the Kenyon cell axons impacts the olfactory
214 responses in the γ-lobes, we calculated the normalized peak fluorescence signal in each
215 compartment of the γ-lobes. We found no differential responses in $\Delta F/F_0$ amplitude to food odour
216 across different compartments of the mushroom body or between 2P and 3P excitation of
217 GCaMP6s (Fig. 4g-4i, Supplementary Fig. 4a). Using a full-compressed imaging preparation, we
218 also imaged the Kenyon cell body responses to odour stimulation and were able to manually
219 distinguish single cell Ca^{2+} traces on a given imaging plane (Supplementary Fig. 4b & 4c).
220 Together, these results suggested that 2P and 3P microscopy with 910 nm and 1320 nm
221 excitation, respectively, are effective in capturing odour evoked Ca^{2+} responses in the mushroom
222 body lobes and cell bodies through the intact head cuticle, and achieve temporal resolution
223 comparable to 2P microscopy with the open cuticle preparations [42].

224 **3P imaging of neural activity captures odour evoked responses of Kenyon cells for 12 hours**

225 Studying how neural circuits change activity during learning or in alternating behavioural states
226 requires non-invasive chronic imaging methods that permit recording neural activity over long time
227 scales. Leveraging the non-invasive nature of our preparation, we pushed the limits of functional

228 imaging of the fly brain in response to odour stimulation to longer time scales (12 hours). Using
229 our custom odour delivery system, we stimulated the fly antenna with apple cider vinegar in ~10
230 minute sessions every four hours while imaging through the head cuticle using our 3P microscope
231 (Fig. 5a). To determine the absolute signal level during long-term imaging, we first calculated the
232 photon counts for representative trials at each time point from the mushroom body γ2 compartment.
233 The photon counts per pixel per second had magnitudes above baseline similar to previously
234 reported levels for 3P excitation of GCaMP6s protein in the mouse brain [23] (Supplementary Fig. 5).
235 Next, we analysed the average odour responses per fly in each γ-lobe compartment and time
236 point (Fig. 5b-5e). We calculated the normalized peak fluorescent signal and the area under the
237 normalized fluorescence curve, as metrics representing the odour response strength and persistence
238 during chronic imaging, respectively. Our analysis showed that the evoked response to food odour
239 did not change with food and water deprivation in any of the imaged γ-lobe compartments (Fig. 5f).
240 However, the persistence of the odour evoked Ca^{2+} response in all of the γ-lobe compartments
241 increased as the experiment progressed (Fig. 5g). We especially noticed a change at 4 hours after
242 the first odour trial, which may reflect a critical state change in the nervous system. Flies continued
243 to show robust calcium responses for at least 4 hours after the change in dynamics (Fig. 5b-5e).
244 During these long-term imaging experiments, we captured the fly's behaviour in parallel
245 with the odour stimulation to assure that the fly stayed alive during long-term imaging
246 (Supplementary Fig. 6). We also checked for heat induced damage after 3P imaging in flies using
247 HSP70 protein as a marker for stress response in glial cells and neurons [43, 44]. We first tested
248 whether HSP70 protein levels reflect heat induced stress response in the fly brain by placing flies in
249 a 30°C incubator for 10 minutes and staining for HSP70 protein right after the incubation. Flies that
250 were kept at room temperature had low levels of the HSP70 protein in a very small number of
251 neurons in the brain (Supplementary Fig. 7a). In contrast, placing flies in a 30°C incubator for 10
252 minutes caused a significant increase in the number of HSP70 positive neurons and an elevation of

253 HSP70 protein levels across the fly brain (Supplementary Fig. 7b). Next, we tested whether 3P
254 imaging causes a heat induced stress response in fly neurons. Head-fixed flies in a semi-
255 compressed imaging prep were imaged for 10 minutes using 3P excitation at 1320nm. we chose to
256 use 10 minutes because this is the total amount of imaging time per time point during our chronic
257 functional imaging experiments. Our results showed that there was no obvious tissue damage or
258 heat-stress response detected by the HSP70 protein levels at the average power levels that we used
259 for functional imaging experiments (~20mW) (Supplementary Fig. 7c). However, increasing laser
260 power (~25mW) caused structural abnormalities and a significant increase in HSP70 protein levels
261 in the fly brain (Supplementary Fig. 7d). These results suggested that 3P non-invasive imaging of
262 the fly brain is safe at lower power levels we used in our experiments, and the non-invasive
263 imaging preparation developed here allows recording of neural activity within an individual fly
264 over long-time scales, which was previously not possible with commonly used open-cuticle
265 preparations.

266 **Discussion**

267 Plasticity in neural states and the ability to learn and remember relevant information are hallmarks
268 of nervous systems, and allow animals to adapt and respond to dynamic environments.
269 Investigating how physiological states, sleep, and learning change the function of neural circuits
270 requires tracking the activity of molecularly defined sets of neurons over long time scales. These
271 experiments require non-invasive imaging methods to record neural activity *in vivo*. In this study,
272 we extensively analysed the fly cuticle by measuring its ballistic and total transmission efficiency
273 across different laser wavelengths. Our results showed that the fly cuticle transmits long
274 wavelength light with high efficiency (Fig. 1). Surprisingly, the transmission at 915 nm
275 wavelength, which is used for 2P microscopy, is only slightly lower than 1320 nm, which is used
276 for 3P excitation of GFP and GCaMP. Based on these results, we investigated the use of 2P and 3P
277 microscopy for non-invasive anatomical imaging of the fly brain. We showed that both 2P and 3P

278 microscopy can be used for non-invasive imaging of fly brain structure and function (Fig. 2-4).
279 While 3P imaging appeared to have higher contrast than 2P imaging, we did not see noticeable
280 difference in the recorded activity traces when performing simultaneous 2P and 3P functional
281 imaging of the mushroom body. We also showed that the tissues interfering with the transmission
282 of the 2P and 3P excitation light during in-vivo imaging are the air sacs located between the head
283 cuticle and the brain, rather than the head cuticle itself (Supplementary Fig. 1). By compressing the
284 fly head to a glass coverslip, we flatten this heterogenous tissue, which increases the transmission
285 of laser light and therefore allows high resolution, non-invasive imaging of the fly brain structures.
286 The non-invasive imaging method developed here also significantly extends the time frame
287 of current *in vivo* imaging preparations used for anatomical and functional studies in fly
288 neuroscience. Non-invasive imaging of the fly brain will allow us to capture the activity of neural
289 populations during changing behavioural states; facilitate decoding of neural plasticity during
290 memory formation; and permit observation of changes in brain structures during development and
291 aging. Our first application of long-term functional imaging of the fly brain captures food odour
292 responses from mushroom body γ-lobes, for the first time up to 12 hours. Our results suggest that
293 odour evoked Ca^{2+} responses gradually change during the repeated odour stimulation. In these
294 chronic imaging experiments, we aimed to image odour responses specifically from γ-lobe
295 compartments. However, because γ and β lobes are very close to each other in depth, some of the
296 fluorescence Ca^{2+} signal we have captured might have been pooled from both of these mushroom
297 body medial lobes. Further experiments using more specific drivers for γ or β lobes will aim to
298 understand the specific location and origins of the change in Ca^{2+} signals and the mechanisms that
299 mediate it. While our focus here was to develop non-invasive in vivo structural and functional
300 imaging methods that can extend imaging length for fly neuroscience research, we anticipate that
301 there will be a wide variety of uses for this technology in *Drosophila* and in other insect models
302 including mosquitoes.

303 **Methods**

304 **Fly stocks**

305 Flies were maintained on conventional cornmeal-agar-molasses medium at 23-25°C and 60-70%
306 relative humidity, under a 12hr light: 12hr dark cycle (lights on at 9 A.M.). Fly strains and sources:
307 *Mef2-GAL4.247* (Bloomington # 50742); *GMR15B07-GAL4* (Bloomington # 48678), *10XUAS-*
308 *IVS-mCD8::GFP* (Bloomington # 32186); *20XUAS-IVS-GCaMP6s* (Bloomington # 42746).

309 **Detailed genotypes of all fly strains used in the paper are as follows**

310 ***Fig. 1***

311 *Males, w^{1118}/Y; 10XUAS-IVS-mCD8::GFP; Mef2-GAL4.*

312 ***Fig. 2***

313 *Males, w^{1118}/Y; 10XUAS-IVS-mCD8::GFP; Mef2-GAL4.*

314 ***Fig. 3***

315 *Panel a, c: Males, w^{1118}/Y; 10XUAS-IVS-mCD8::GFP; Mef2-GAL4.*

316 *Panel d-g: Males, w^{1118}/Y; 10XUAS-IVS-mCD8::GFP; GMR15B07-GAL4.*

317 ***Fig. 4 & 5***

318 *Males, w^{1118}/Y; 20XUAS-IVS-GCaMP6s; Mef2-GAL4.*

319 ***Supplementary Fig. 1***

320 *Males, w^{1118}/Y; 20XUAS-IVS-GCaMP6s; Mef2-GAL4.*

321 ***Supplementary Fig. 2***

322 *Males, w^{1118}/Y;10XUAS-IVS-mCD8::GFP;GMR15B07-GAL4.*

323 ***Supplementary Fig. 3***

324 *Panel a, Males, w^{1118}/Y; 10XUAS-IVS-mCD8::GFP; Mef2-GAL4*

325 *Panel b, Males, w^{1118}/Y;10XUAS-IVS-mCD8::GFP;GMR15B07-GAL4.*

326 ***Supplementary Fig. 4-7***

327 *Males, w^{1118}/Y; 20XUAS-IVS-GCaMP6s; Mef2-GAL4.*

328 **Optical transmission measurements of the fly head cuticle**

329 Drosophila cuticle was dissected from the dorsal head capsule of flies that are age and gender
330 controlled (male, 5 days old). The dissected cuticle was sandwiched between two #1.5 coverslips
331 with UV curable resin to avoid dehydration of the sample (Fig. 1a). Measurements from each
332 dissected cuticle was done within a day. The first few measurements were repeated at the end of all
333 measurements to ensure that dehydration or protein degradation, which may vary the optical
334 properties of the tissue, did not happen as the experiment progressed. The total transmission and
335 ballistic transmission of cuticle samples were measured using a custom-built device (Fig. 1b). For
336 ballistic transmission experiments, we assume collimated light passes through the sample since the
337 Rayleigh range for a 25 μm ($1/e^2$) focus spot is ~1mm - 2mm (λ = 1630 nm – 852 nm), which is
338 much larger than the thickness of the whole coverslip sandwich-prep. The transmitted light from
339 the cuticle was coupled to a single mode fibre with identical focusing optics to measure its ballistic
340 transmission. A photodetector was used to monitor the power fluctuation during the measurement
341 and thus to ensure identical incident power (~10mW) on the cuticle in each measurement. An
342 infrared camera was used to image the sample and incident beam to ensure the incident light spot is
343 always on the cuticle and to avoid very dark pigments (usually at the edge of the cuticle), ocelli,
344 and possible cracks introduced during dissection. The ballistic transmission of the cuticle was then
345 calculated as the optical power ratio between the ballistic transmissions of the cuticle and the
346 surrounding areas without the cuticle, containing only the UV curable resin (i.e., the reference)
347 using the equation below (SMF = single mode fibre, T = transmission, T_o= reference transmission):

348 $$T_{ballistic} = \frac{T^{SMF}}{T_0^{SMF}}$$

349 For total transmission experiments, we assume collimated light passes through the sample since the
350 Rayleigh range for a 50 μm ($1/e^2$) spot size is ~5mm - 10mm (λ = 1630 nm – 532 nm), which is
351 much larger than the thickness of the whole coverslip sandwich-prep. A photodetector was used to
352 monitor the power fluctuation during the measurement. The incident power on the sample is

353 ~10mW. An infrared camera was setup to visualize the light spot and the cuticle when the
354 integrating sphere is removed. The cuticle was translated to obtain measurements at different
355 locations. The total transmission of the cuticle was then calculated as the optical power ratio
356 between the transmissions of the cuticle and the surrounding areas without the cuticle, containing
357 only the UV curable resin (i.e., the reference) measured by the integrating sphere (IS = integrating
358 sphere, T = transmission, T_o= reference transmission).

359 $$T_{total} = \frac{T^{IS}}{T_0^{IS}}$$

360 **Laser sources**

361 Excitation source (Fig. 2-5, Supplementary Fig 1,2 &3-5): The excitation source is a wavelength-
362 tuneable optical parametric amplifier (OPA, Opera-F, Coherent) pumped by a femtosecond laser
363 with a MOPA (Master Oscillator Power Amplifier) architecture (Monaco, Coherent). A prism pair
364 (10SF10, Newport) and a silicon wafer are used to compensate for the dispersion of the optics of
365 the light source and the microscope including the objective, for 1320 nm. The laser repetition rate
366 is maintained at 1 MHz for both structural and functional imaging.

367 Excitation source (Supplementary Fig. 3): The alternative laser used as the excitation source for 3P
368 microscopy is an optical parametric amplifier (OPA, KM Labs), pumped by the KM Labs Y-
369 Fi™HP. A two-prism glass compressor (SF 10 glass) is used to compensate for the normal
370 dispersion of the optics of the light source and the microscope. The Y-Fi™ OPA has an operating
371 wavelength centred at 1300 nm and outputs average power of ~400 mW (1 MHz repetition rate).
372 Pulse duration is less than 150 fs. Power control of the laser was achieved using a half wave plate
373 (HWP) (Thorlabs) and a polarizing beam splitter cube (PBS) (Thorlabs) and ScanImage module for
374 MATLAB (Mathworks).

375 **Multiphoton microscopes**

376 Imaging setup (Fig. 2-5, Supplementary Fig. 1,2 & 4,5): The images were acquired with a custom-
377 built multiphoton microscope. The scan lens is a C-coated achromat (AC254-030-C-ML, Thorlabs)

378 for high transmission at 1320 nm, and the transmission of the tube lens (Sutter Instrument) is 82%.
379 For imaging experiments that use GFP and GCaMP6s, we used a custom high numerical aperture
380 (NA) water immersion microscope objective (Olympus XLPLN25XWMP2, 25X, NA 1.05), which
381 is specially coated for high transmission (~70%) at 1320 nm. 2 detection channels were used to
382 collect the fluorescence signal and the third harmonic generation (THG) signal by photomultiplier
383 tubes (PMT) with GaAsP photocathode (H7422-40, Hamamatsu). For GFP and GCaMP6s imaging
384 at 1320 nm, fluorescence signal and THG signal were selected by a 520/60 nm band-pass filter
385 (FF01-520/60-25, Semrock) and a 435/40 nm band-pass filter (FF02-435/40-25, Semrock),
386 respectively. For signal sampling, the PMT current is converted to voltage and low-pass-filtered
387 (200 kHz) by a transimpedance amplifier (C7319, Hamamatsu). Analog-to-digital conversion is
388 performed by a data acquisition card (NI PCI- 6110, National Instruments). ScanImage 5.4 (Vidrio
389 Technologies) running on MATLAB (MathWorks) was used to acquire images and control a 3D
390 translation stage to move the sample (MP-285, Sutter Instrument Company). All imaging depths
391 and thickness are reported in raw axial movement of the motorized stage, unless otherwise stated.
392 Imaging setup (Supplementary Fig. 3): Images were acquired using a custom-built multiphoton
393 microscope with a pair of galvanometric scanners (Cambridge Technology). The objective used
394 was a high numerical aperture water immersion objective (Olympus XLPLN25XWMP2, 25X, NA
395 1.05). Signal from specimens was collected through the objective and then reflected by multiple
396 dichroic beam splitters. (FF520-Di02- 25 x 36, Semrock, and FF484-Di01- 25 x 36, Semrock) to
397 the detectors. The two-channel detection system consists of a green fluorescence signal and third
398 harmonic generation (THG). ScanImage was used to control the ILS100CC motorized translation
399 stage (Newport). High-resolution structural images were typically taken with 512x512
400 pixels/frame, 0.24 Hz frame rate, and multiple frame averages at each depth.

401 **Non-invasive *in vivo* imaging preparation**

402 All animals used for imaging experiments were male flies with indicated genotypes kept in 25ºC
403 incubators and maintained on conventional cornmeal-agar-molasses medium. Flies used for chronic
404 functional experiments were 2-7 days old, and flies used for short term functional experiments were
405 1-4 days old. To perform intact brain imaging, flies were first head-fixed in a 40 mm weigh dish
406 (VWR#76299-236) with a hole made with forceps. A drop of UV curable resin (Liquid plastic
407 welder, Bondic®) was applied to the head and thorax, which was then cured with blue light (~470
408 nm) and fused to a cover glass. Fly proboscises were immobilized with blue light curable resin to
409 minimize head motion caused by muscle contractions. Only flies in Supplementary Fig. 1 went
410 through surgery to remove the air sacs using a sharp needle.

411 **Odour delivery**

412 Food odour, apple cider vinegar, was delivered using a custom built olfactometer as described
413 previously [45]. Clean room air was pumped (Active Aqua Air Pump, 4 Outlets, 6W, 15 L/min) into
414 the olfactometer, and the flow rate was regulated by a mass flow controller (Aalborg GFC17). Two
415 Arduino controlled 3-way solenoid valves (3-Way Ported Style with Circuit Board Mounts,
416 LFAA0503110H) controlled air flow. One valve delivered the odourised airstream either to an
417 exhaust outlet or to the main air channel, while another valve directed air flow either to the
418 stimulus or control channel. The stimulus channel contained a 50 ml glass vial containing undiluted
419 apple cider vinegar (volume=10 ml) (Wegmans), while the control channel contained a 50 ml glass
420 vial containing mineral oil (volume=10 ml). For odour stimulation experiments, flies were placed
421 approximately 1 cm from a clear PVC output tube (OD = 1.3 mm, ID = 0.84 mm), which passed a
422 ~1< L/min air stream to the antennae. The odour stimulus latency was calculated before the
423 experiments using a photo ionization detector (PID) (Aurora Scientific). We sampled odour
424 delivery using the PID every 20 ms and found average latency to peak odour amplitude was <
425 100ms across 34 measurements.

426 **Simultaneous 2P and 3P Structural and Functional Imaging**

427 Simultaneous imaging with 2P excitation and 3P excitation is achieved by temporal multiplexing of
428 the 910- nm Ti:Sapphire laser and 1,300- nm Spirit-NOPA laser (Fig. 4 and Supplementary Fig.4):
429 They were spatially overlapped at the same focal position after the objective. The 910- nm laser
430 was intensity modulated with an electro-optic modulator (EOM), switching it on for ~1 μs between
431 two adjacent Spirit-NOPA laser pulses. The EOM is driven by a radio frequency signal triggered
432 by the Spirit-NOPA pulse train so that the sample is alternatively illuminated either with 910- nm
433 laser for 2P excitation or 1,320- nm laser for 3P excitation. By recording the NOPA pulses and the
434 PMT signal at 5 MHz sampling rate (200 ns pixel time), the 2P and 3P excited fluorescence signals
435 can be temporally demultiplexed with a postprocessing MATLAB script.

436 For short term functional imaging, flies were food deprived for 16-24 hours in vials with a
437 wet Kim wipe. Each odour stimulation trial consisted of 50 seconds of clean mineral oil, 3 seconds
438 of undiluted apple cider vinegar stimulus, and another 50 seconds of mineral oil. Between trials,
439 scanning was stopped for 20 seconds to minimize the risk of imaging-induced tissue stress. Five
440 trials were performed sequentially.

441 **3P Chronic Functional Imaging**

442 Flies used in long term functional imaging experiments were fed 100 mM sucrose just before the
443 first trial to assure that the flies were in a fed state. Each odour stimulation trial consisted of 50
444 seconds of clean mineral oil, 3 seconds of undiluted apple cider vinegar stimulus, and another 50
445 seconds of mineral oil. Between trials, scanning was stopped for 20 seconds. The images were
446 captured at 256x512 pixel resolution and 2.13 Hz frame rate. Five trials were performed
447 sequentially and the five-trial block was repeated every four hours. Between trial blocks, scanning
448 was stopped, and air passing through the stimulation tube was redirected to the exhaust valve to
449 prevent desiccation. To further prevent desiccation, flies were placed on a water-absorbing polymer
450 bead. Fly behaviour was videotaped from the side to capture any movement by a CCD camera

451 (FLIR, Blackfly S, BFS-U3-13Y3M-C) equipped with a 1.5-megapixel macro lens (Computar,
452 COM MLM3X-MP, 3X Macro Zoom). We captured fly behaviour with videos at 4.3 Hz speed
453 using the Spinnaker SDK (Flir) image acquisition software under IR light illumination.

454 **Photon counting**

455 To show the absolute signal strength in the unit of photon count rate, pixel values are multiplied by
456 a calibration factor, which is obtained by taking the ratio of the photon count rate with a photon
457 counter (SR400, Stanford Research Systems) and the average pixel value, simultaneously recorded
458 on a uniform fluorescein sample (Supplementary Fig. 5).

459 **Immunohistochemistry for brain tissue damage assessment**

460 To investigate laser-induced stress in the brain during 3-photon imaging through the intact head
461 cuticle, 1-2-day old male homozygous MB>GCaMP6s flies were imaged continually at 1320 nm
462 for 10 minutes. The laser was focused 70μm below the cuticle with ~20mW or ~25mW average
463 power. Flies were head compressed and fed 100mM sucrose before imaging to reproduce actual
464 experimental conditions. Laser exposed brains were dissected approximately 2 hours after
465 mounting. To test HSP70 antibody efficacy on fly brains, a positive control group of flies was first
466 exposed to 30°C for 10 minutes in an incubator to induce HSP70 expression. Negative control
467 group of flies was kept at room temperature. For whole mount staining, brains were dissected in
468 phosphate-buffered saline (PBS) and incubated in 4% paraformaldehyde (PFA) in PBS for 20-30
469 minutes at room temperature on an orbital shaker. Tissues were washed 3-4 times over 1 hour in
470 PBS (calcium- and magnesium-free; Lonza BioWhittaker #17-517Q) containing 0.1% Triton X-
471 100 (PBT) at room temperature. Samples were blocked in 5% Normal Goat Serum in PBT (NGS-
472 PBT) for 1 hour and then incubated with primary antibodies diluted in NGS-PBT for 24 hours at
473 4°C. Primary antibodies used were anti-GFP (Torrey Pines, TP40, rabbit polyclonal, 1:1000), anti-
474 BRP (DSHB, nc82, mouse monoclonal, 1:20), and anti-HSP70 (Sigma, SAB5200204, rat
475 monoclonal, 1:200). The next day, samples were washed 5-6 times over 2 hours in PBT at room

476 temperature and incubated with secondary antibodies (Invitrogen) diluted in NGS-PBT for 24
477 hours at 4°C. On the third day, samples were washed 4-6 times over 2 hours in PBT at room
478 temperature and mounted with VECTASHIELD Mounting Media (Vector Labs, Burlingame, CA,
479 USA) using glass slides between two bridge glass coverslips. The samples were covered by a glass
480 coverslip on top and sealed using clear nail polish. Images were acquired at 1024x1024 pixel
481 resolution at ~1.7 μm intervals using an upright Zeiss LSM 880 laser scanning confocal microscope
482 and Zeiss digital image processing software ZEN. Maximum projection images of Z-stacks were
483 generated in the ZEN image-processing software. The power, pinhole size and gain values were
484 kept the same for all imaged brains during confocal microscopy.

485 **Data analysis**

486 Resolution measurements: We measured the lateral brightness distribution of small features within
487 the GFP labelled fly brains (Fig. 3f) and the THG signal (Fig. 3g), which sets an upper bound on
488 the lateral resolution value. Lateral intensity profiles measured along the white lines were fitted by
489 a Gaussian profile for the estimation of the lateral resolution.

490 Image processing for structural imaging. TIFF stacks containing fluorescence data were converted
491 to 8 bits. When necessary, stacks were registered using the TurboReg plugin in ImageJ. Images
492 shown in Fig. 3 are an average of 3 z-stacks spanning 3 microns. 3D reconstructions of the z-stacks
493 were generated using the Imaris v9.2, Bitplane Inc., software available at http://bitplane.com.
494 Images shown in Supplementary Fig. 2 are an average of single z sections at different depths.

495 Image processing for activity recordings. TIFF stacks containing fluorescence data were converted
496 to 32 bits, and pixel values were left unscaled. When necessary, stacks were registered using the
497 TurboReg plugin in ImageJ. Images acquired during the multiplexed 2p-3p imaging sessions were
498 first median filtered with a filter radius of 10 pixels to reduce high amplitude noise. To compute
499 $\Delta F/F_0$ traces, γ-lobe ROIs were first manually selected using a custom Python script. F_0 was
500 computed as the average of 10 frames preceding stimulus onset. The F_0 image was then subtracted

501 from each frame, and the resulting image was divided by F_0. The resulting trace was then low-pass
502 filtered by a moving mean filter with a window size of 2 frames (8 frames for multiplexed activity
503 data). Data were analysed using Python (code available upon request) and plotted in Microsoft
504 Excel. Peak $\Delta F/F_0$ was determined by the peak value within 20 frames after the odour delivery. We
505 measured the persistence as the total area under the normalized curve after the peak $\Delta F/F_0$ value. To
506 prevent underestimating persistence as a result of negative values in the $\Delta F/F_0$ trace, values that
507 followed a zero-crossing were set to zero. Averaged traces were manually inspected for each lobe
508 and trial block, and rejected if peak $\Delta F/F_0$ was lower than the noise detected in the entire trial.
509 These traces had lower than 0.1 peak $\Delta F/F_0$ value. These accounted for less than 15% of the total
510 trials in 3 flies tested for chronic imaging.
511 Fly movement analysis: Fly motion traces were obtained using the DeepLabCut tracking program
512 [46]. To train the network, we manually annotated movement in the fly bodies and legs for 340
513 frames across multiple cropped and contrast-enhanced videos. The data shown in Supplementary
514 Fig. 6 shows the activity of front tarsi or hind legs.

515 **Statistical analysis**

516 All statistical analyses were performed using Prism V8.0.1 (GraphPad). Data collected in
517 functional imaging experiments are shown as mean ± SEM. Details of statistical methods are
518 reported in the Fig. legends. Statistical significance in chronic imaging across time points and in
519 different mushroom body compartments was determined with a two-way repeated measures
520 ANOVA. In all of the figures, plots labelled with different letters are significantly different from
521 each other.

522 **Acknowledgements**

523 We thank Joe Fetcho, Andy Bass, David Owald, and members of the Yapici Lab for comments on
524 the manuscript. We acknowledge Bloomington Drosophila Stock Centre (NIH P40OD018537) and
525 the Developmental Studies Hybridoma Bank (NICHD of the NIH, University of Iowa) for reagents.
526 We thank Li Yan McCurdy (Yale University) and Matt Einhorn (Cornell University) for help with
527 the design and construction of the custom built olfactometer, Elena Zhong for training the neural
528 network for behavioural analysis in Deep Lab Cut, Joe Fetcho (Cornell University) for help with
529 Imaris software, and Nancy M. Bonini (University of Pennsylvania) for her advice on the HSP70
530 antibody. Research in N.Y.'s laboratory is supported by a Cornell University Nancy and Peter
531 Meinig Family Investigator Program, a Pew Biomedical Scholar Award, the Alfred P. Sloan
532 Foundation Award, AFAR Research Grant for Junior Faculty, NSF NeuroNex Program Grant
533 (DBI-1707312), and NIH R35 ESI-MIRA Grant (R35GM133698-01).

534 **Author contributions**

535 The authors have made the following declarations about their contributions: Conceived and
536 supervised the study: C.X., and N.Y. Designed the experiments: M.J.A, M.W., J.S., A.M., C.X.,
537 and N.Y. Performed the experiments: J.S., N.B., and A.M. (Fig. 1, Supplementary Fig. 1), M.J.A.,
538 and M.W. (Fig. 2-5, Supplementary Fig. 2 -6), K.L. (Supplementary Fig. 3), H.K. (Supplementary
539 Fig. 7). Analysed the data and prepared Figures: M.J.A., M.W, J.S., A.M. and N.Y. Wrote the
540 paper: N.Y. with input from C.X., M.J.A., M.W., C.S., J.S., A.M., K.L., and H.K.

541 **Competing financial interests**

542 The authors declare no competing financial interests.

543 **Data availability**

544 All raw imaging data supporting the findings of this study are available from the corresponding
545 author on request.

546 **References**

547 1. Tinbergen, N. The study of instinct. (Oxford University Press, Oxford; 1969).

548 2. Nevin, J.A. The study of behavior : learning, motivation, emotion, and instinct. (Scott,
549 Foresman, Glenview, IL; Brighton; 1973).

550 3. Hunt, L.T. & Hayden, B.Y. A distributed, hierarchical and recurrent framework for reward-
551 based choice. *Nat Rev Neurosci* **18**, 172-182 (2017).

552 4. Dickson, B.J. Wired for sex: the neurobiology of Drosophila mating decisions. *Science* **322**,
553 904-909 (2008).

554 5. McFarland, D.J. Decision making in animals. *Nature* **269**, 15-21 (1977).

555 6. Lutcke, H., Margolis, D.J. & Helmchen, F. Steady or changing? Long-term monitoring of
556 neuronal population activity. *Trends Neurosci* **36**, 375-384 (2013).

557 7. Lerner, T.N., Ye, L. & Deisseroth, K. Communication in Neural Circuits: Tools,
558 Opportunities, and Challenges. *Cell* **164**, 1136-1150 (2016).

559 8. Luo, L., Callaway, E.M. & Svoboda, K. Genetic Dissection of Neural Circuits: A Decade of
560 Progress. *Neuron* **98**, 256-281 (2018).

561 9. Svoboda, K. & Yasuda, R. Principles of two-photon excitation microscopy and its
562 applications to neuroscience. *Neuron* **50**, 823-839 (2006).

563 10. Ji, N., Freeman, J. & Smith, S.L. Technologies for imaging neural activity in large volumes.
564 *Nat Neurosci* **19**, 1154-1164 (2016).

565 11. Yapici, N., Zimmer, M. & Domingos, A.I. Cellular and molecular basis of decision-making.
566 *EMBO Rep* **15**, 1023-1035 (2014).

567 12. Barron, A.B., Gurney, K.N., Meah, L.F., Vasilaki, E. & Marshall, J.A. Decision-making and
568 action selection in insects: inspiration from vertebrate-based theories. *Front Behav Neurosci* **9**, 216
569 (2015).

570 13. Simpson, J.H. & Looger, L.L. Functional Imaging and Optogenetics in Drosophila. *Genetics*
571 **208**, 1291-1309 (2018).

572 14. Grover, D., Katsuki, T. & Greenspan, R.J. Flyception: imaging brain activity in freely
573 walking fruit flies. *Nat Methods* **13**, 569-572 (2016).

574 15. Minocci, D., Carbognin, E., Murmu, M.S. & Martin, J.R. In vivo functional calcium imaging
575 of induced or spontaneous activity in the fly brain using a GFP-apoaequorin-based bioluminescent
576 approach. *Biochim Biophys Acta* **1833**, 1632-1640 (2013).

577 16. Sinha, S. et al. High-speed laser microsurgery of alert fruit flies for fluorescence imaging of
578 neural activity. *Proc Natl Acad Sci U S A* **110**, 18374-18379 (2013).

579 17. Seelig, J.D. et al. Two-photon calcium imaging from head-fixed Drosophila during optomotor
580 walking behavior. *Nat Methods* **7**, 535-540 (2010).

581 18. Wang, J.W., Wong, A.M., Flores, J., Vosshall, L.B. & Axel, R. Two-photon calcium imaging
582 reveals an odor-evoked map of activity in the fly brain. *Cell* **112**, 271-282 (2003).

583 19. Trachtenberg, J.T. et al. Long-term in vivo imaging of experience-dependent synaptic
584 plasticity in adult cortex. *Nature* **420**, 788-794 (2002).

585 20. Hefendehl, J.K. et al. Repeatable target localization for long-term in vivo imaging of mice
586 with 2-photon microscopy. *J Neurosci Methods* **205**, 357-363 (2012).

587 21. Huang, C. et al. Long-term optical brain imaging in live adult fruit flies. *Nat Commun* **9**, 872
588 (2018).

589 22. Wang, M. et al. Comparing the effective attenuation lengths for long wavelength in vivo
590 imaging of the mouse brain. *Biomed Opt Express* **9**, 3534-3543 (2018).

591 23. Wang, T. et al. Three-photon imaging of mouse brain structure and function through the intact
592 skull. *Nat Methods* **15**, 789-792 (2018).

593 24. Horton, N.G. et al. In vivo three-photon microscopy of subcortical structures within an intact
594 mouse brain. *Nat Photonics* **7** (2013).

595 25. Ouzounov, D.G. et al. In vivo three-photon imaging of activity of GCaMP6-labeled neurons
596 deep in intact mouse brain. *Nat Methods* (2017).

597 26. Tao, X. et al. Transcutical imaging with cellular and subcellular resolution. *Biomed Opt*
598 *Express* **8**, 1277-1289 (2017).

599 27. Chen, T.W. et al. Ultrasensitive fluorescent proteins for imaging neuronal activity. *Nature*
600 **499**, 295-300 (2013).

601 28. Strausfeld, N.J., Hansen, L., Li, Y., Gomez, R.S. & Ito, K. Evolution, discovery, and
602 interpretations of arthropod mushroom bodies. *Learn Mem* **5**, 11-37 (1998).

603 29. Crittenden, J.R., Skoulakis, E.M., Han, K.A., Kalderon, D. & Davis, R.L. Tripartite
604 mushroom body architecture revealed by antigenic markers. *Learn Mem* **5**, 38-51 (1998).

605 30. Ito, K. et al. The organization of extrinsic neurons and their implications in the functional
606 roles of the mushroom bodies in Drosophila melanogaster Meigen. *Learn Mem* **5**, 52-77 (1998).

607 31. Yagi, R., Mabuchi, Y., Mizunami, M. & Tanaka, N.K. Convergence of multimodal sensory
608 pathways to the mushroom body calyx in Drosophila melanogaster. *Sci Rep* **6**, 29481 (2016).

609 32. Owald, D. & Waddell, S. Olfactory learning skews mushroom body output pathways to steer
610 behavioral choice in Drosophila. *Curr Opin Neurobiol* **35**, 178-184 (2015).

611 33. Lin, Y.Y. et al. Three-wavelength light control of freely moving Drosophila Melanogaster
612 for less perturbation and efficient social-behavioral studies. *Biomed Opt Express* **6**, 514-523 (2015).

613 34. Zheng, Z. et al. A Complete Electron Microscopy Volume of the Brain of Adult Drosophila
614 melanogaster. *Cell* **174**, 730-743 e722 (2018).

615 35. Krashes, M.J., Keene, A.C., Leung, B., Armstrong, J.D. & Waddell, S. Sequential use of
616 mushroom body neuron subsets during drosophila odor memory processing. *Neuron* **53**, 103-115
617 (2007).

618 36. Hsu, K.J., Lin, Y.Y., Chiang, A.S. & Chu, S.W. Optical properties of adult Drosophila brains
619 in one-, two-, and three-photon microscopy. *Biomed Opt Express* **10**, 1627-1637 (2019).

620 37. Barad, Y., Eisenberg, H., Horowitz, M. & Silberberg, Y. Nonlinear scanning laser
621 microscopy by third harmonic generation. *SPIE milestone series* **175**, 47-49 (2003).

622 38. Wolff, T., Iyer, N.A. & Rubin, G.M. Neuroarchitecture and neuroanatomy of the Drosophila
623 central complex: A GAL4-based dissection of protocerebral bridge neurons and circuits. *J Comp*
624 *Neurol* **523**, 997-1037 (2015).

625 39. Pfeiffer, K. & Homberg, U. Organization and functional roles of the central complex in the
626 insect brain. *Annu Rev Entomol* **59**, 165-184 (2014).

627 40. Seelig, J.D. & Jayaraman, V. Neural dynamics for landmark orientation and angular path
628 integration. *Nature* **521**, 186-191 (2015).

629 41. Xie, X. et al. The laminar organization of the Drosophila ellipsoid body is semaphorin-
630 dependent and prevents the formation of ectopic synaptic connections. *Elife* **6** (2017).

631 42. Cohn, R., Morantte, I. & Ruta, V. Coordinated and Compartmentalized Neuromodulation
632 Shapes Sensory Processing in Drosophila. *Cell* **163**, 1742-1755 (2015).

633 43. Podgorski, K. & Ranganathan, G. Brain heating induced by near-infrared lasers during
634 multiphoton microscopy. *J Neurophysiol* **116**, 1012-1023 (2016).

635 44. Lindquist, S. Varying patterns of protein synthesis in Drosophila during heat shock:
636 implications for regulation. *Dev Biol* **77**, 463-479 (1980).

637 45. Raccuglia, D. et al. Presynaptic GABA Receptors Mediate Temporal Contrast Enhancement
638 in Drosophila Olfactory Sensory Neurons and Modulate Odor-Driven Behavioral Kinetics. *eNeuro*
639 **3** (2016).

640 46. Mathis, A. et al. DeepLabCut: markerless pose estimation of user-defined body parts with
641 deep learning. *Nat Neurosci* **21**, 1281-1289 (2018).

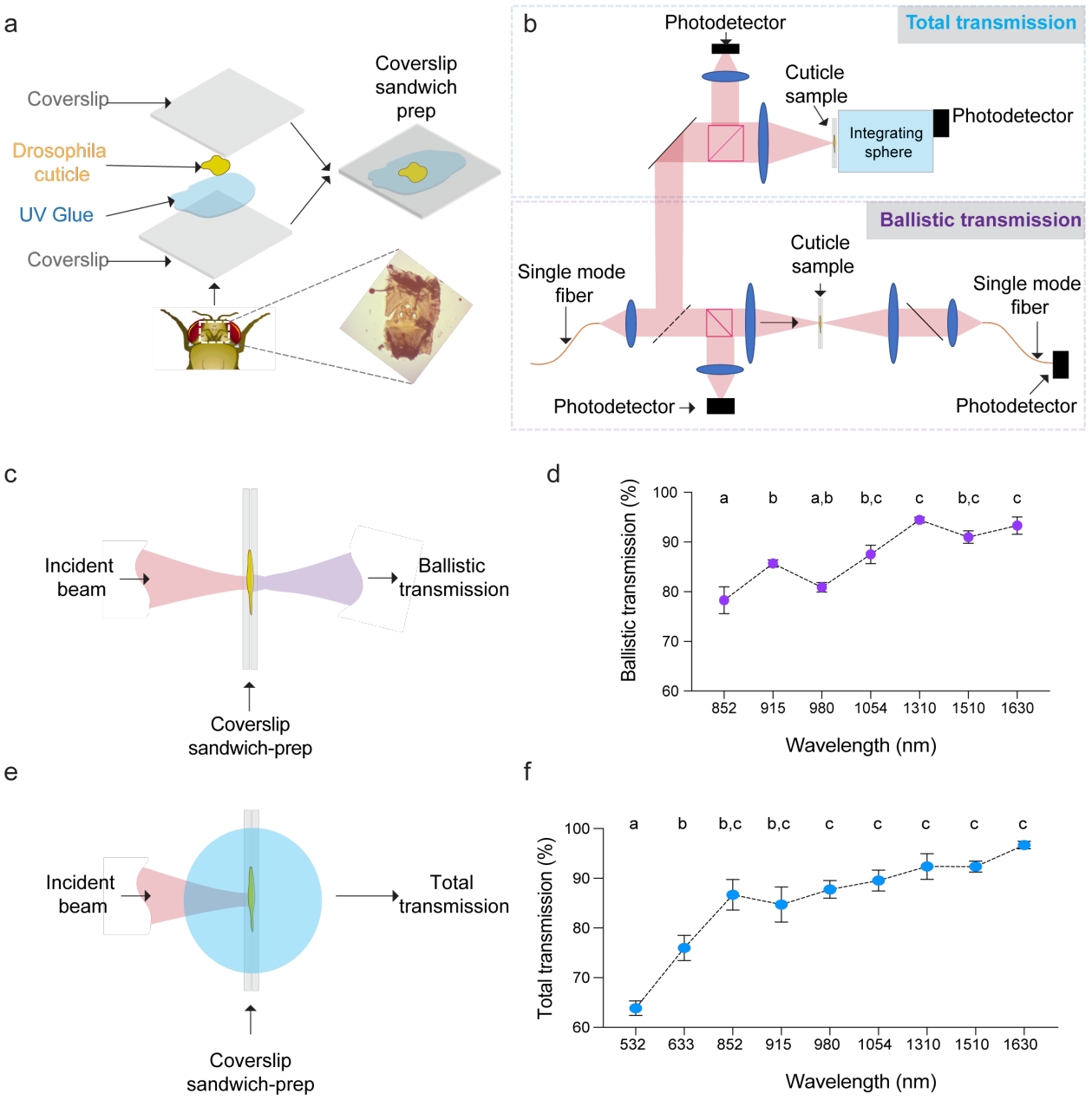

Fig. 1: Ballistic and total optical transmission of the fly head cuticle. a, Schematic of the cuticle transmission preparation. Fly head cuticle is dissected and placed in UV curable resin between two cover slips. **b,** Schematic of the cuticle optical transmission measurement setup. **c,** Schematic of the ballistic optical transmission through the cuticle. **d,** Results of the ballistic optical transmission experiments across various wavelengths (the mean and standard error of mean of all measurements (n = 56 at each wavelength) from 5 different cuticle samples). **e,** Schematic of the total optical transmission through the cuticle. **f,** Results of the total optical transmission experiments across various wavelengths (the mean and standard error of mean of all measurements (n = 20 at each wavelength) from 5 different cuticle samples). ANOVA with post-hoc Tukey's test was conducted to compare transmission at different wavelengths ($p<0.001$).

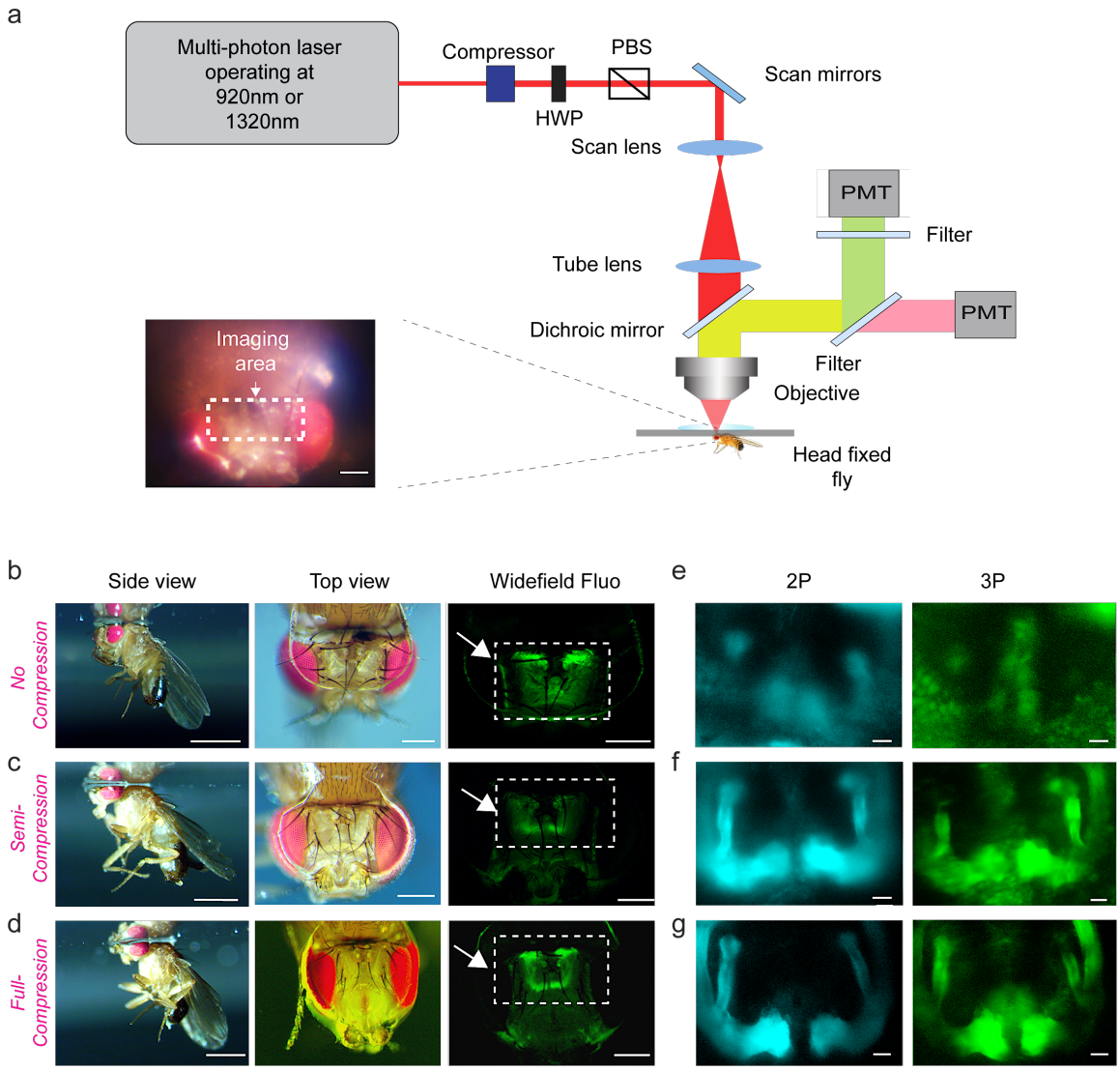

Fig. 2. **Non-invasive imaging of the fly brain with 2P and 3P excitation. a,** Schematic of the multiphoton microscope setup. Fly head is fixed to a cover slip and placed under the objective (HWP: half-wave plate, PBS: polarization beam splitter, PMT: photomultiplier tube). The imaging window on the fly head is shown in the picture (lower left). **b-d**, The uncompressed and compressed imaging preparations. The first column shows the side image of the fly that is head fixed to the cover glass (scale bar =1mm). The second and third columns show the uncompressed and compressed fly head visualized under a brightfield (top view) and fluorescent dissecting microscopes (widefield-fluo), respectively. Arrows and the rectangle area in Widefield-Fluo column indicate the imaging window (scale bar=200µm). **e-g,** Cross section imaging of the mushroom body (MB) Kenyon cells expressing CD8-GFP through the head cuticle at 910 nm (2P) and 1320 nm (3P) excitation. The Z projections of 2P (cyan, left) and 3P (green, right) imaging stacks. For each imaging preparation, the same fly head is imaged with 3P excitation and 2P excitation (scale bar=20µm).

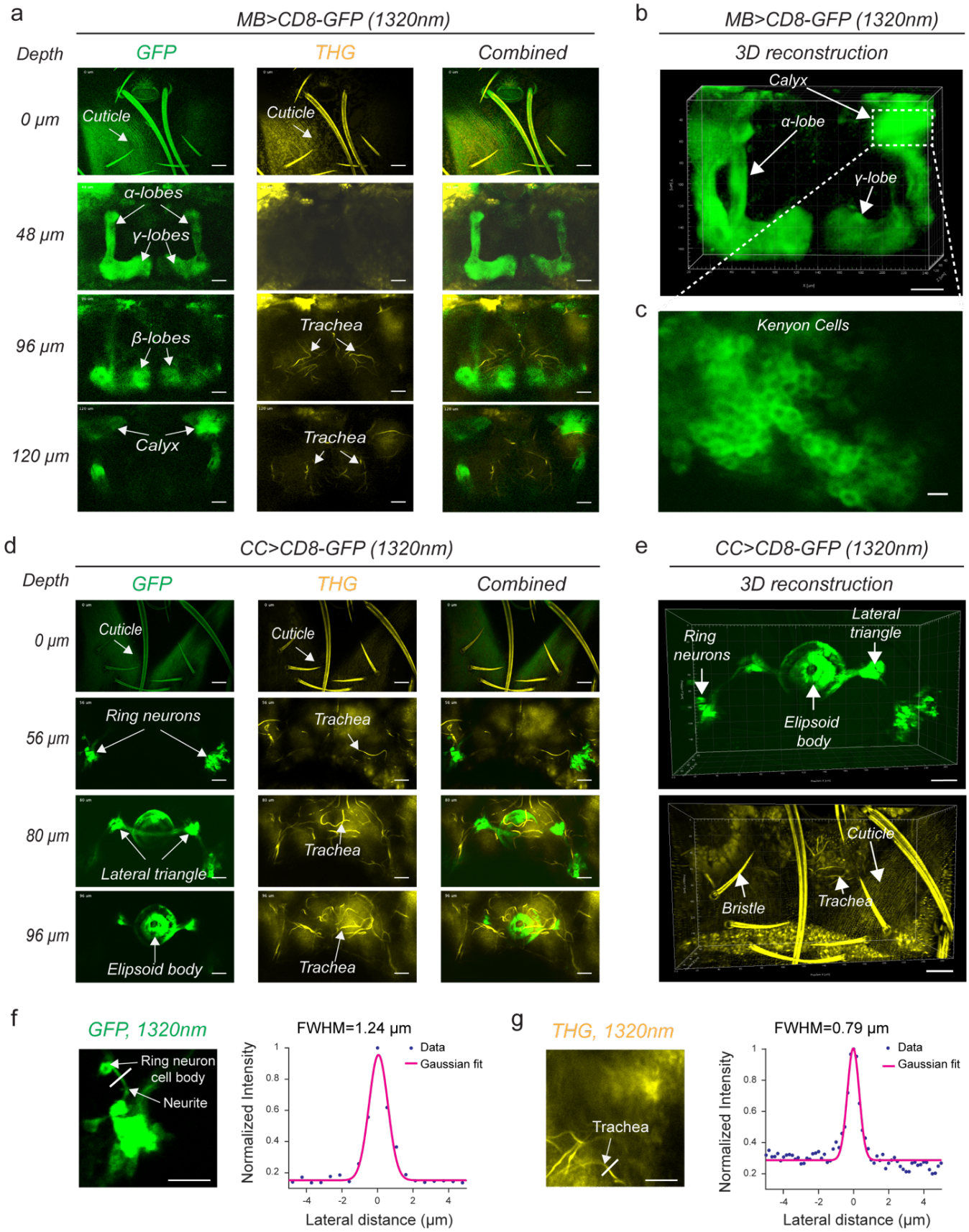
a
MB>CD8-GFP (1320nm)
Depth
GFP
THG
Combined
0 µm
48 µm
96 µm
120 µm
Cuticle
α-lobes
γ-lobes
β-lobes
Calyx
Trachea
b
MB>CD8-GFP (1320nm)
3D reconstruction
Calyx
α-lobe
γ-lobe
c
Kenyon Cells
d
CC>CD8-GFP (1320nm)
Depth
GFP
THG
Combined
0 µm
56 µm
80 µm
96 µm
Cuticle
Ring neurons
Trachea
Lateral triangle
Elipsoid body
e
CC>CD8-GFP (1320nm)
3D reconstruction
Ring neurons
Lateral triangle
Elipsoid body
Cuticle
Bristle
Trachea
f
GFP, 1320nm
Ring neuron cell body
Neurite
FWHM=1.24 µm
Data
Gaussian fit
Normalized Intensity
Lateral distance (µm)
g
THG, 1320nm
Trachea
FWHM=0.79 µm
Data
Gaussian fit
Normalized Intensity
Lateral distance (µm)

Fig. 3. High resolution 3P structural imaging of the mushroom body and the central complex neurons through the cuticle with 1320 nm excitation. a, Cross section images of the mushroom body (MB) lobes through the cuticle with 3P excitation at 1320 nm (green). Third harmonic generation (THG) imaging visualizes the tracheal arbours (yellow). White arrows indicate different MB compartments that are identified (scale bars= 30 µm, semi-compressed prep). **b**, 3D reconstruction of the z-stack images in 3A (scale bars= 30 µm). **c,** Kenyon cell bodies that are located around the calyx (scale bar= 5 µm, compressed prep.) **d,** Cross section imaging of the central complex (CC) ring neurons through the cuticle with 1320 nm excitation (green). Third harmonic generation (THG) imaging visualizes the tracheal arbours (yellow). Arrows indicate different CC compartments that are identified. **e,** 3D reconstruction of the z stack images in 3c, GFP (upper panel) and THG (lower panel) (scale bars= 30 µm, semi-compressed prep). **f,** The GFP profile of CC ring neurons (green) and **g,** the THG profile of surrounding trachea (yellow). Lateral intensity profiles measured along the white lines are fitted by a Gaussian profile for the lateral resolution estimation (scale bars=20 µm, semi-compressed prep).

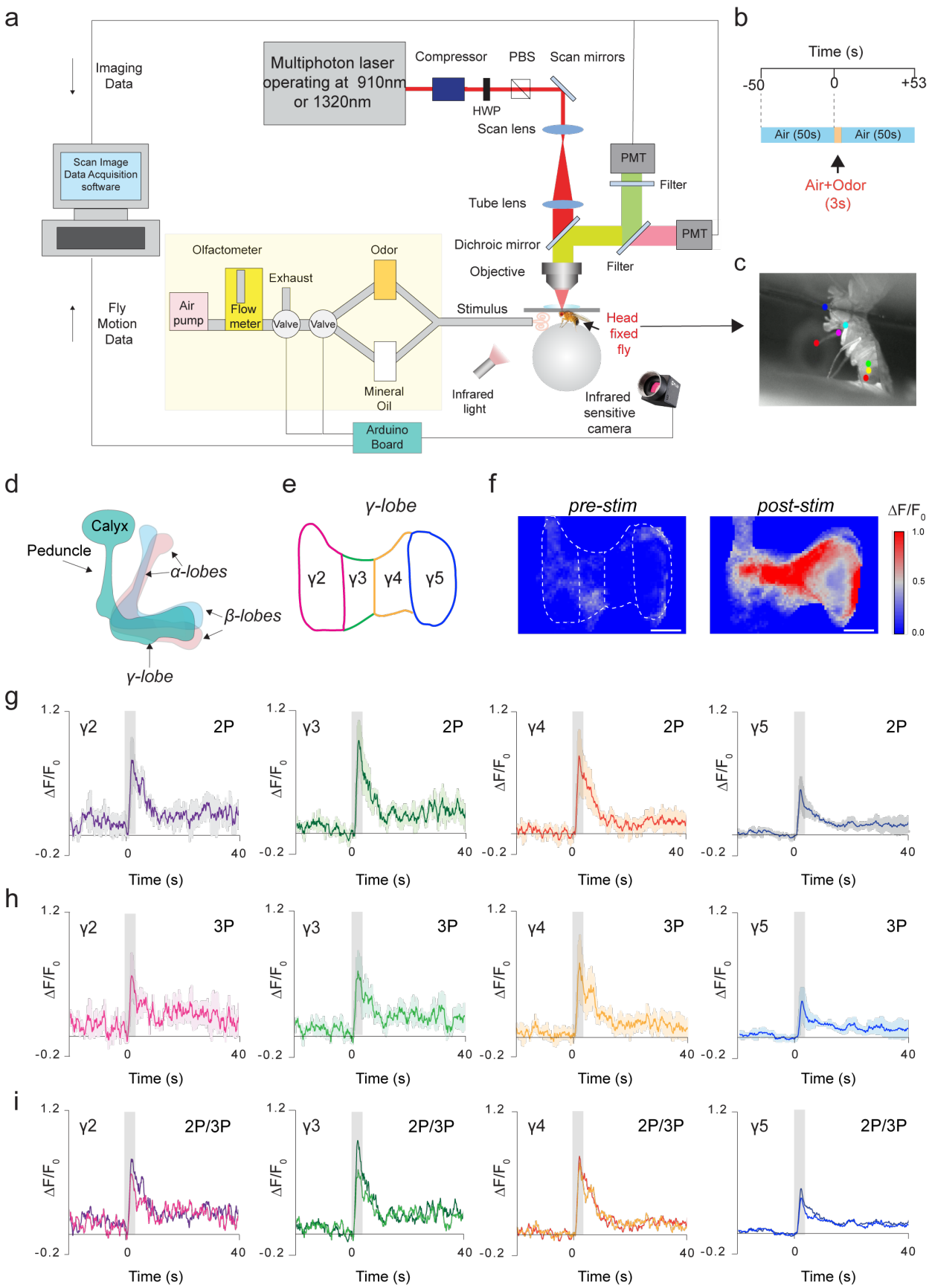
a
Imaging Data
Multiphoton laser operating at 910nm or 1320nm
Compressor
PBS
Scan mirrors
HWP
Scan lens
Scan Image Data Acquisition software
PMT
Filter
Tube lens
Dichroic mirror
PMT
Filter
Objective
Olfactometer
Odor
Exhaust
Air pump
Flow meter
Valve
Valve
Stimulus
Head fixed fly
Fly Motion Data
Mineral Oil
Infrared light
Infrared sensitive camera
Arduino Board
b
Time (s)
-50
0
+53
Air (50s)
Air (50s)
Air+Odor (3s)
c
d
Calyx
Peduncle
α-lobes
β-lobes
γ-lobe
e
γ-lobe
γ2
γ3
γ4
γ5
f
pre-stim
post-stim
ΔF/F0
1.0
0.5
0.0
g
γ2
γ3
γ4
γ5
2P
ΔF/F0
1.2
-0.2
0
40
Time (s)
h
γ2
γ3
γ4
γ5
3P
i
γ2
γ3
γ4
γ5
2P/3P

679 **Fig. 4. Simultaneous 2P and 3P functional imaging of short-term odour-evoked responses of**
680 **the mushroom body Kenyon cells. a,** Schematic of the custom made olfactometer. This
681 olfactometer is used to puff odours to the fly that is placed on a ball for functional Ca^{2+} imaging
682 using GCaMP6s and a semi-compressed imaging prep. An Arduino board synchronizes the FLIR
683 Black Fly S Camera to capture fly behaviour. ScanImage software is used to capture images from
684 temporally multiplexed 2P (910nm) and 3P (1320nm) excitation at 160x165 pixel resolution
685 (described in detail in the methods). **b,** Stimulus timeline. Flies were stimulated with air (50s),
686 before and after the odour stimulus (odour + air, 3s). Each trial lasted 103s. Flies were stimulated 5
687 times using the same odour stimulus scheme. **c,** Picture of the head fixed fly on the ball under the
688 3-photon microscope. The coloured dots show the body parts that were tracked and used to train the
689 DeepLabCut neural network. **d,** Schematic of the mushroom body anatomy indicating the location
690 of α, β, and γ lobes. **e,** γ-lobes have discrete anatomical compartments (shown as $\gamma 2$–$\gamma 5$). **f,**
691 GCaMP6s is expressed in the mushroom body Kenyon cells. Normalized ($\Delta F/F_0$) GCaMP6s signal
692 is shown before (left) and after (right) odour stimulus (scale bar= 20 μm). **g,** Odour-evoked
693 responses of Kenyon cells captured by 2P excitation at 910 nm and **h,** 3P excitation at 1320 nm. **i,**
694 Comparison of 2P and 3P average responses over time (n=3 flies, 4-5 trials per fly, data are
695 presented as mean ± SEM in **g** and **h,** grey bar indicates when stimulus is present).

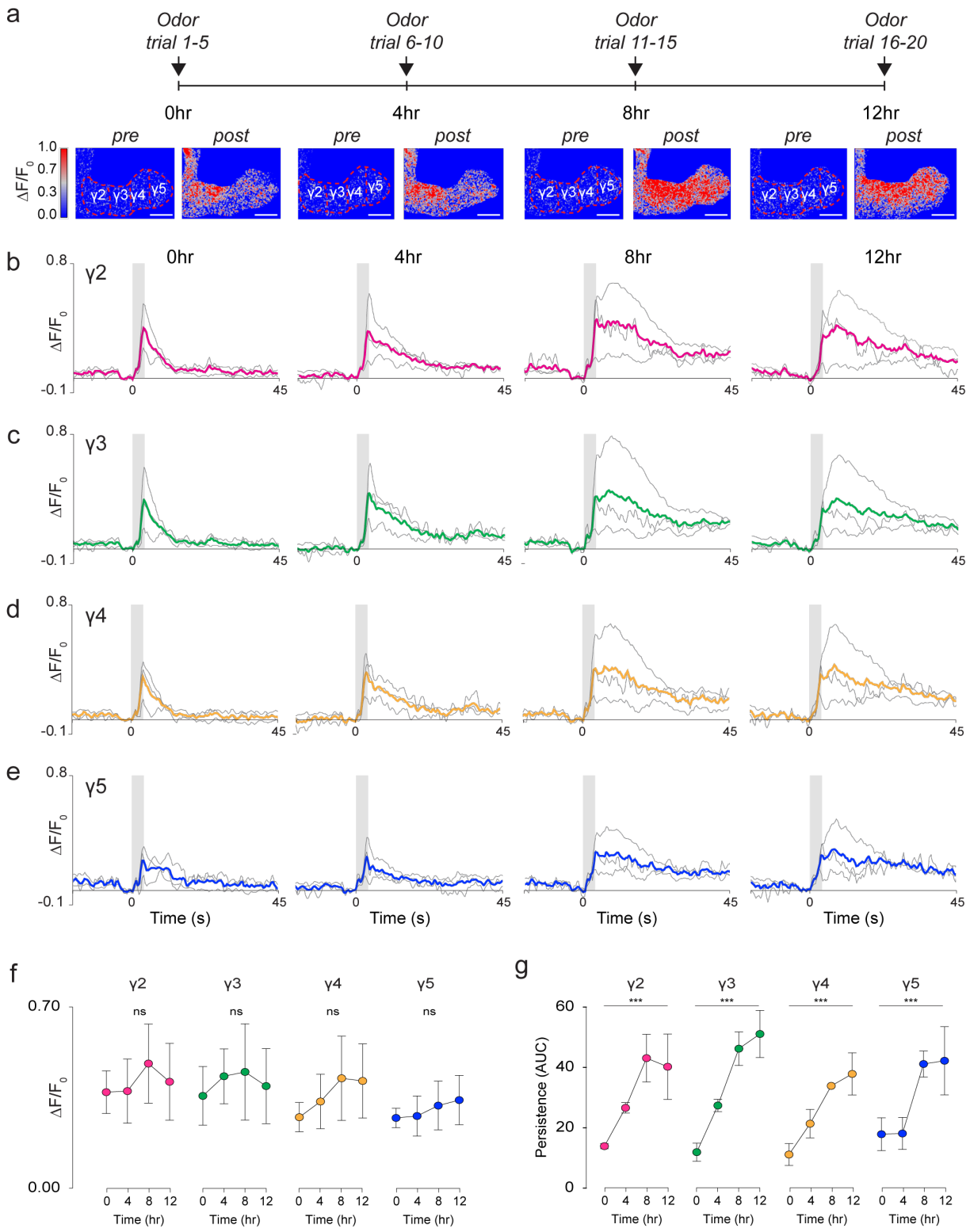
a
Odor trial 1-5
Odor trial 6-10
Odor trial 11-15
Odor trial 16-20
0hr
4hr
8hr
12hr
pre
post
ΔF/F0
1.0
0.7
0.3
0.0
γ2 γ3 γ4 γ5
b
γ2
c
γ3
d
γ4
e
γ5
0.8
-0.1
0
45
Time (s)
f
γ2
γ3
γ4
γ5
ns
0.70
0.00
Time (hr)
g
***
Persistence (AUC)
60
40
20
0

696 **Fig. 5. Long-term 3P imaging of odour-evoked responses of the mushroom body Kenyon cells**
697 **a,** Stimulus timeline for chronic odour imaging. GCaMP6s signal is captured from Kenyon cells
698 axons innervating mushroom body γ-lobes using the semi-compressed prep. Normalized $\Delta F/F_0$
699 signal is shown before (left) and after (right) the odour stimulus (scale bar= 20 μm). **b-e,**
700 Quantification of the normalized $\Delta F/F_0$ signal over time in each γ-lobe compartment. Each lobe's
701 response is colour coded differently. Grey bar indicates when the odour stimulus is present. Each
702 grey line indicates the average response of a fly over multiple trials in a given hour. The average
703 response of 3 flies is shown. Each compartment's response is labelled with a different colour. **f,**
704 Quantification of the peak amplitude ($\Delta F_{max}/F_0$). **g,** Area under the curve (AUC) after the odour
705 stimulus for each compartment of the γ-lobes (Two-way repeated measures ANOVA. Data are
706 presented as mean ± SEM, ns= not significant, ***=$p<0.001$, n=3 flies, 3-5 trials per time point).

Supplementary Information

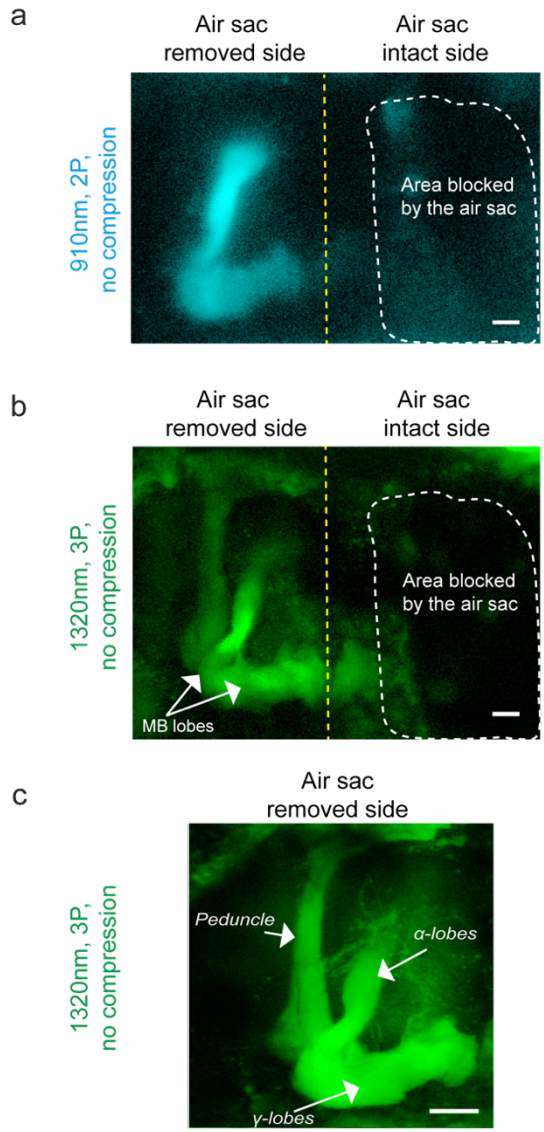

Supp. Fig. 1. Removal of air sacs allows 2P and 3P imaging in an uncompressed prep. Cross section imaging of the mushroom body (MB) Kenyon cells expressing GCaMP6s through the head cuticle at 910 nm (2P) and 1320 nm (3P) excitation after removing air sacs on one side of the head. Head is not compressed to the cover slip **a,** The Z projections of 2P (cyan) and **b,** 3P (green) imaging stacks. For each imaging preparation, the same fly head is imaged with 3P excitation and 2P excitation. Mushroom body structures are visible on the side where air sacs are removed. The dotted lines show the area where the air sacs block imaging. **c,** Higher resolution 3P images taken from the brain side where the air sacs are removed. Mushroom body lobes and peduncle are clearly visible without the head compression. Scale bars = 20µm.

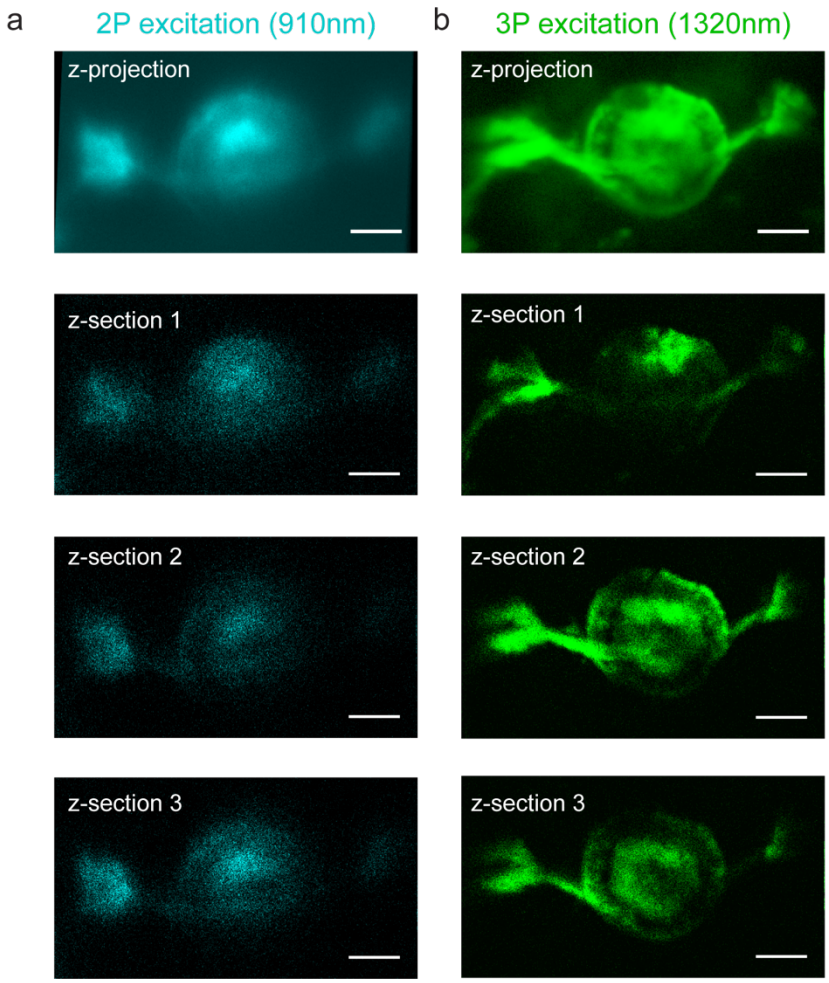

716 **Supp. Fig. 2. Non-invasive imaging of the central complex ring neurons with 2P and 3P**
717 **excitation.** Cross section imaging of the Central Complex (CC) ring neurons expressing CD8-GFP
718 through the head cuticle at 910 nm (2P) and 1320 nm (3P) excitation. **a-b**, The Z projection (top-
719 most) and single optical section images at ~10 µm step of ellipsoid body processes. **a,** 2P (cyan)
720 and **b,** 3P (green) images are shown. For each imaging preparation, the same fly head is imaged
721 with both 3P and 2P excitation. (scale bars=25µm, semi-compressed prep).

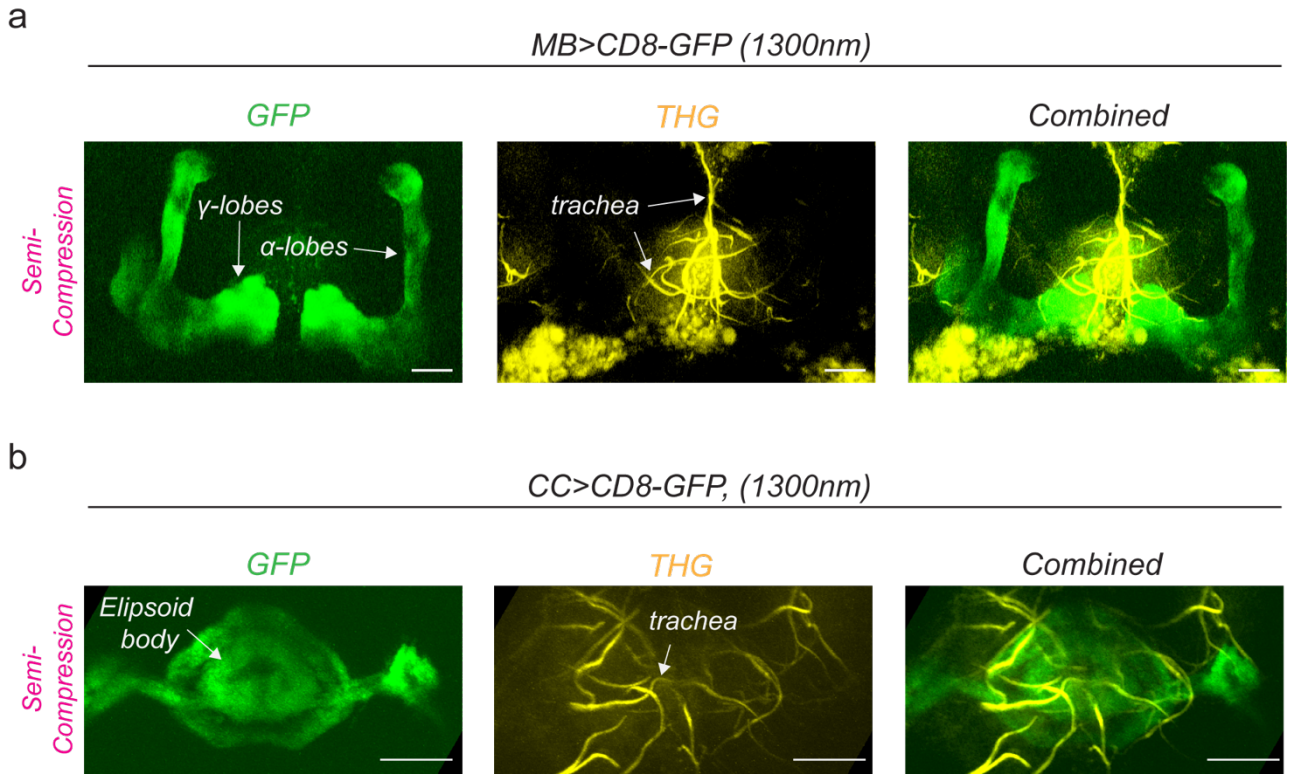

722 **Supp. Fig. 3. 3P structural imaging of the fly brain through the cuticle with 1320 nm using an**
723 **alternative laser source.** Cross section imaging of the fly brain through the cuticle at 1320 nm.
724 **a,** Compressed z-stack images of flies expressing membrane tagged GFP in the Mushroom Body
725 (MB) Kenyon cells (green, right). **b,** Compressed z-stack images of flies expressing membrane
726 tagged GFP in Central Complex (CC) ring neurons (green, right). Third harmonic generation
727 (THG) imaging visualizes the tracheal arbours (yellow). Arrows indicate different MB and CC
728 compartments that are identified with 3P imaging (scale bars= 25µm).

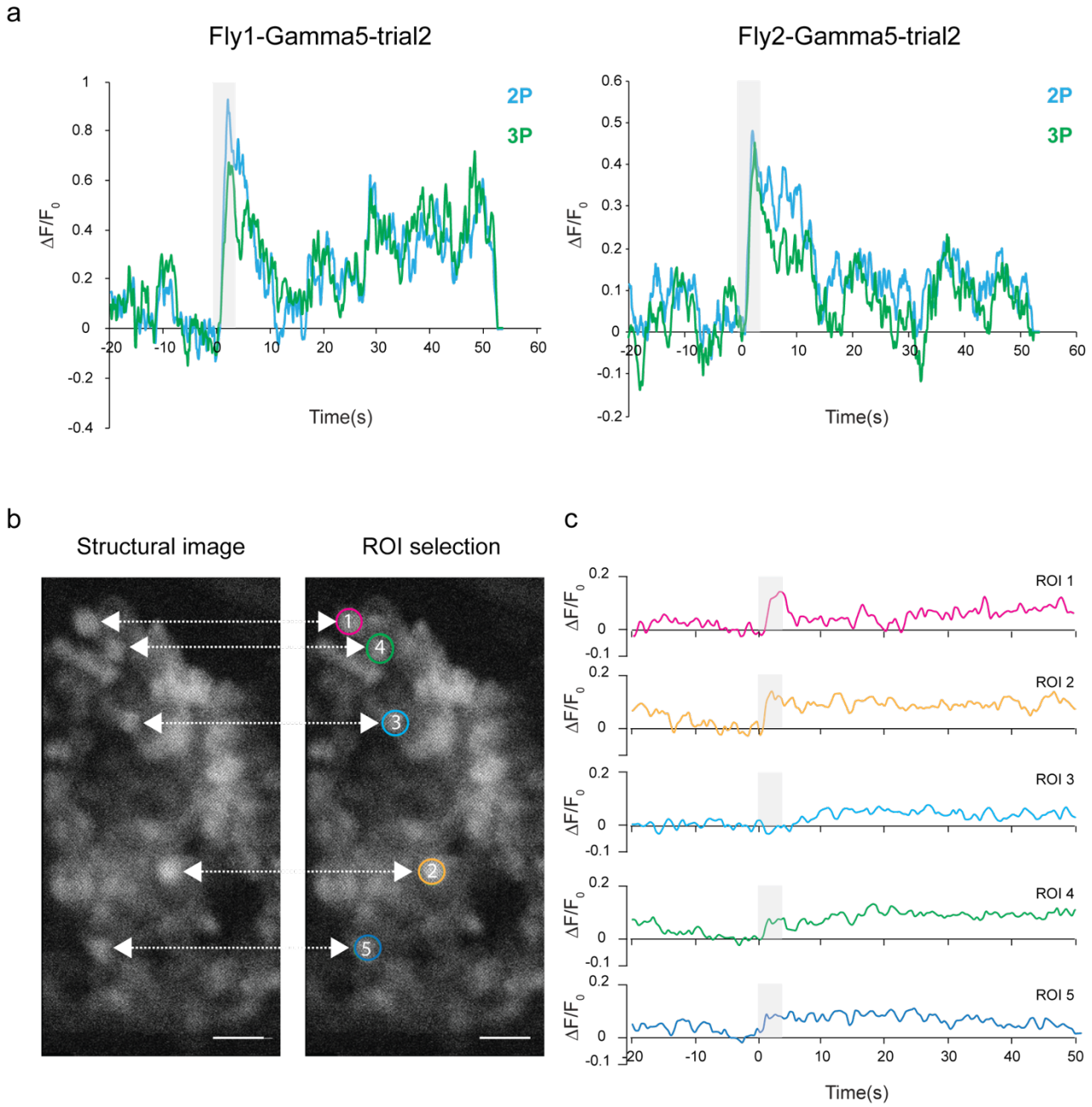

Supp. Fig. 4. Short term 2P and 3P functional imaging of odour-evoked responses of the mushroom body gamma lobes and cell bodies. a, Ca^{2+} imaging of odour responses in gamma lobe compartments. Left and right panels show single trial normalized $\Delta F/F_0$ signal over time using simultaneous 2P (cyan) and 3P (green) excitation from indicated gamma lobe compartments (semi-compression prep). **b,** 3P structural image of the Kenyon cell bodies and ROI selection**. c,** Quantification of the normalized $\Delta F/F_0$ signal over time in 5 ROIs, each corresponding to a Kenyon cell soma imaged with 3P excitation. Grey bar indicates when the odour stimulus is present (scale bars= 10µm, full-compression prep).

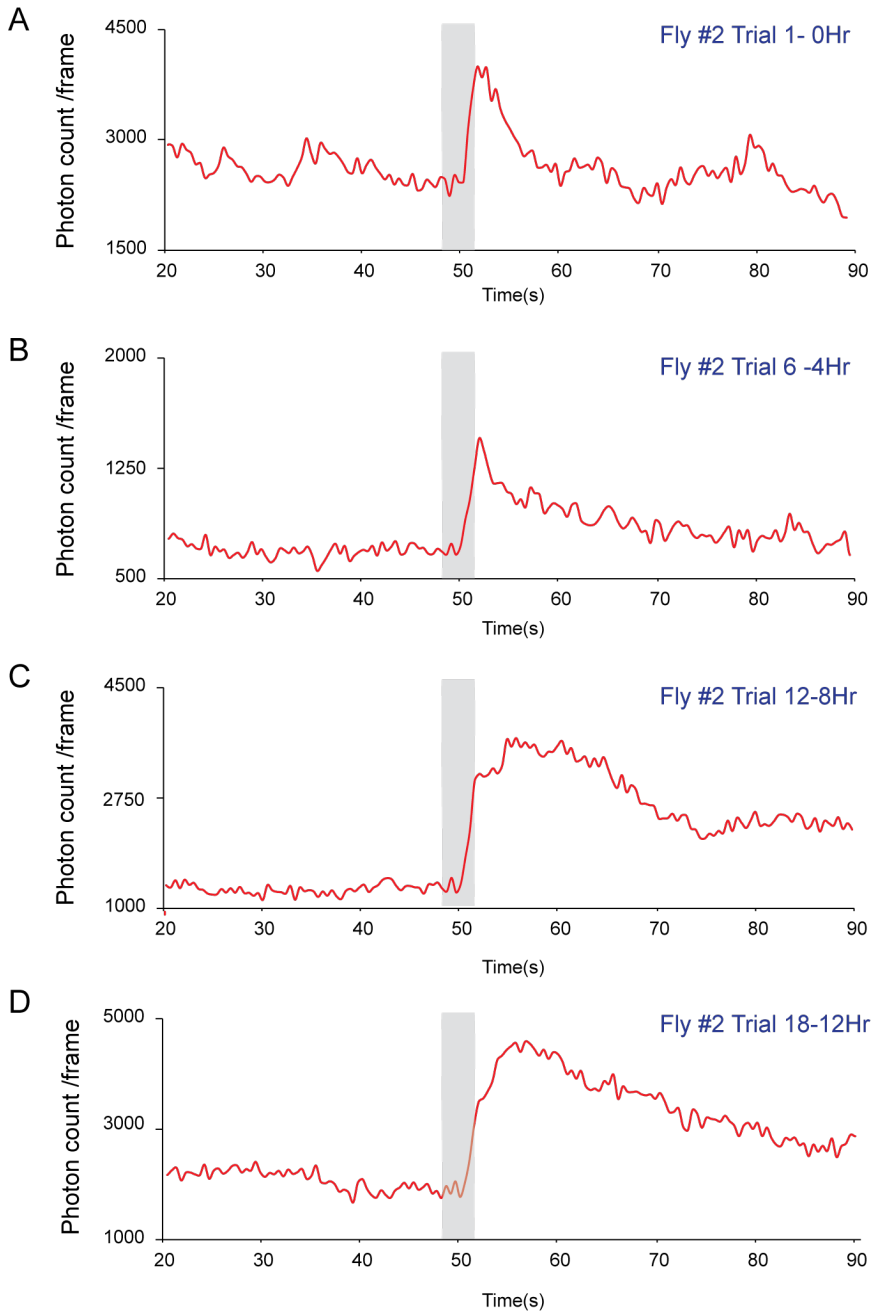

738 **Supp. Fig. 5. Photon counts during 3-photon functional imaging.** Odour-evoked neural activity
739 in GCaMP6s-labeled Kenyon cells forming mushroom body γ-lobes, imaged at average power of
740 ~20 mW and 1 MHz repetition rate. **a-d,** Plots show the activity of the γ2-compartment of the
741 mushroom body in fly#2 in a single trial across different time points. The fluorescence intensity is
742 converted to photon counts per frame in the selected ROI (~50x50 pixels, frame rate=2.13Hz.).

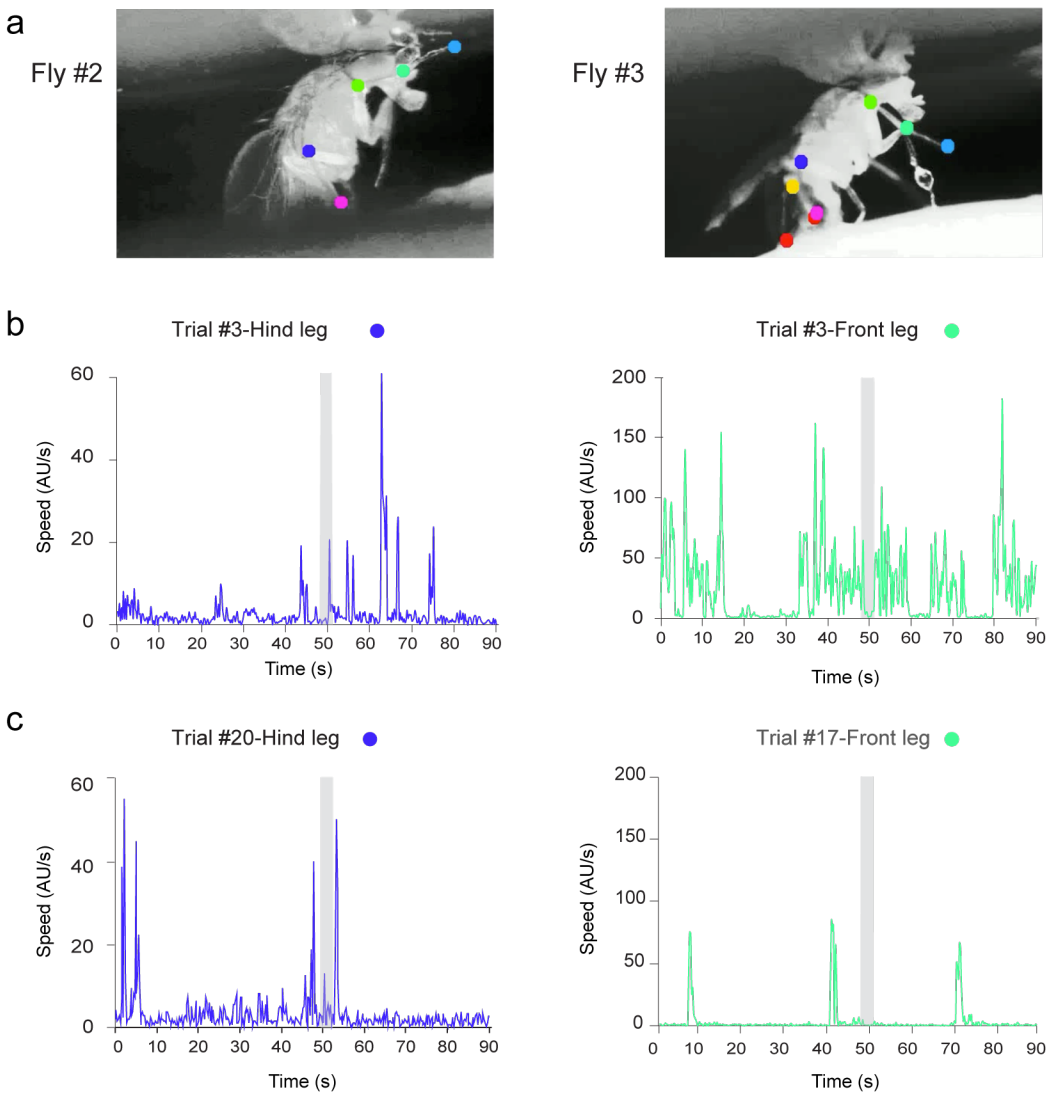

743 **Supp. Fig. 6. Fly motion traces during chronic imaging. a,** Picture of the head fixed fly on the
744 polymer ball under the 3-photon microscope. The coloured dots show the body parts that were
745 tracked and used to train the DeepLabCut neural network. **b-c,** The speed of indicated legs (blue
746 and green) during the odour stimulus trials. Grey bar indicates when the stimulus is present. Speed
747 is calculated as arbitrary units per second (AU/s).

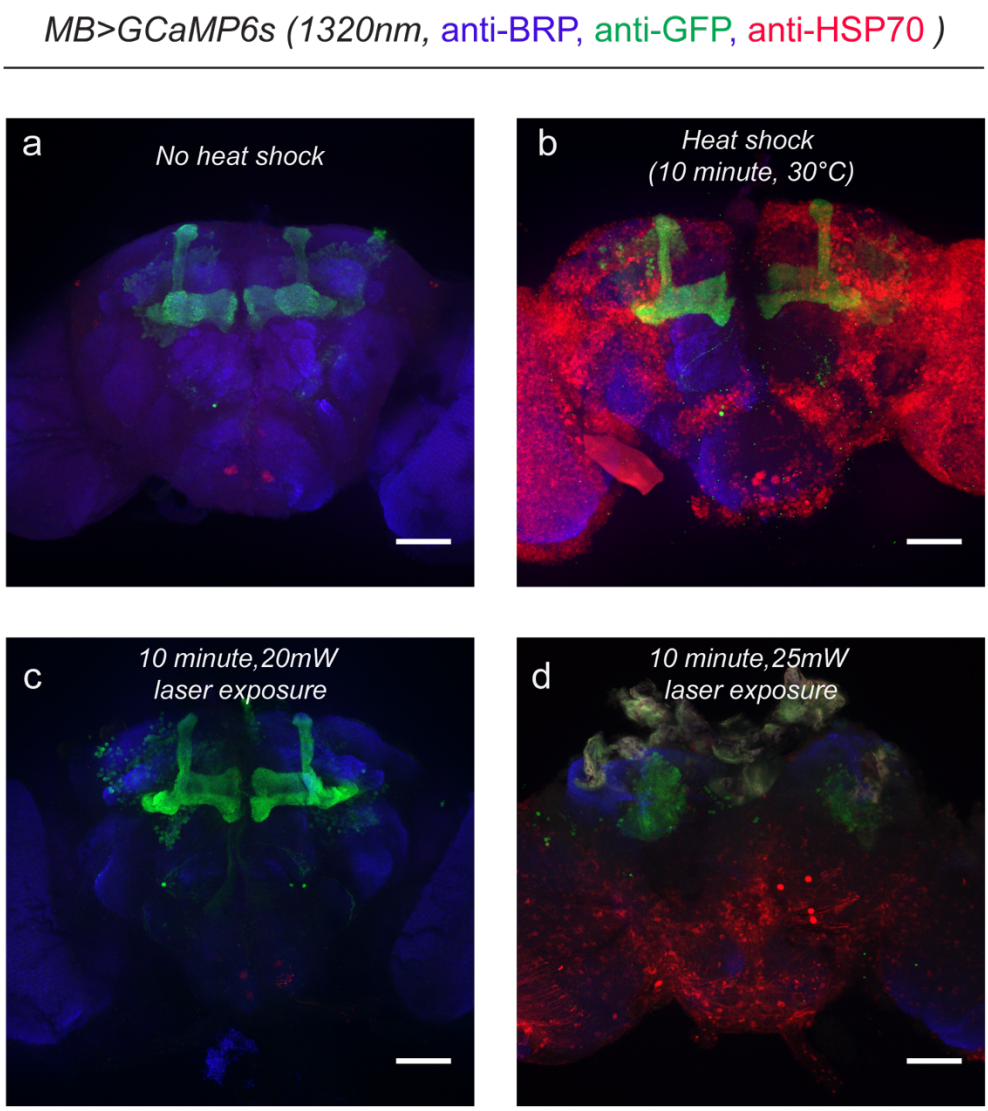

Supp. Fig. 7. HSP70 staining of fly brains shows no heat-induced stress responses after 1320 nm 3P excitation with average power (~20mW) used in functional imaging experiments. a, Without heat shock, there is minimal HSP70 protein expressed in the fly brain. **b,** When flies are exposed to heat (30ºC) for 10 minutes, the HSP70 protein level is significantly elevated across the brain. **c-d**, HSP70 protein expression in the fly brain after 3-photon imaging at 1320 nm for 10 minutes. **c,** There is no obvious change in HSP70 protein levels when power is 20mW. **d,** HSP70 protein expression is significantly elevated when power is 25mW (scale bars= 50 µm). The optical power is measured at the sample plane of the microscope using a power meter (n=2-4 flies per condition).

757

758 **Supp. Video 1: Z stack of the mushroom body (MB) Kenyon cells expressing CD8-GFP.**
759 Cross section imaging through the head cuticle at 1320 nm (3P) excitation (scale bar=20µm,
760 compressed prep).

761

762 **Supp. Video 2: Z stack of the mushroom body (MB) Kenyon cells expressing CD8-GFP.**
763 Cross section imaging through the head cuticle at 910 nm (2P) excitation (scale bar=20µm,
764 compressed prep).

765

766 **Supp. Video 3: Z stack of the mushroom body (MB) Kenyon cells expressing GCaMP6s.**
767 Imaging is done through the head cuticle using 1320 nm (3P) excitation after removing air sacs
768 only on one side of the head (scale bar = 50µm, no compression).

769

770 **Supp. Video 4: Z stack of the ellipsoid body (EB) ring neurons expressing CD8-GFP.**
771 Cross section imaging through the head cuticle at 1320 nm (3P) excitation (scale bar=20µm, semi-
772 compressed prep).

773

774 **Supp. Video 5: 3D reconstruction of Z stacks of the ellipsoid body (EB) ring neurons**
775 **expressing CD8-GFP.** (Green= CD8-GFP, yellow=THG, scale bar= 40 µm, semi-compressed
776 prep).

777

778 **Supp. Video 6: Odour-evoked responses of mushroom body gamma lobes captured from an**
779 **intact fly head through the cuticle.** Functional imaging is performed using a food odour, apple
780 cider vinegar, with 3P excitation at 1320 nm. Video is sped up 10x (semi-compressed prep).